TABLE 3. Proviral load of in vivo infected cells[a]

Mouse	Proviral load (%)	
	Lavage specimen	Spleen
2-wk group		
2W-1	3.7	0.6
2W-2	34.0	1.4
2W-3	2.8	0.5
4-wk group		
4W-1	33.6	14.1
4W-2	48.1	12.9

[a] The percentages of the proviral load, calculated by comparison with a control DNA as described in Materials and Methods are shown for cells recovered from abdominal lavage and cells isolated from spleens of MT-2-inoculated hu-PBMC-NOG mice.

TABLE 4. Proviral load in $CD4^+$ and $CD8^+$ T cells[a]

Mouse	Proviral load (%)	
	$CD4^+$	$CD8^+$
2-wk group		
2W-1	0.6	0.7
2W-2	4.5	1.1
2W-3	1.2	0.4
4-wk group		
4W-1	14.9	7.8
4W-2	19.9	13.6

[a] Human $CD4^+$ and $CD8^+$ T cells were purified from 10^7 splenocytes of mice sacrificed at 2 or 4 weeks p.i. with the use of magnetic beads. Proviral load was determined by real-time PCR as described in Materials and Methods.

ment of the HTLV-1 pX region by using PCR, and proviral DNA was detected in the cells recovered from the MT-2-inoculated groups of hu-PBMC-NOG mice (data not shown). These PCR products were not derived from contamination of cellular DNA of MT-2 cells, since a PCR specific for one of HTLV-1 integration sites in MT-2 did not detect the provirus (data not shown). Splenocytes tended to have a lower proviral load than cells recovered from the peritoneal cavity. However, the proviral load in the 4-week group was generally greater than that from the 2-week group, suggesting the continuous proliferation of infected cells and propagation of the virus in this mouse model (Table 3).

Significant increase in the memory $CD4^+$ T-cell population after HTLV-1 infection. Although HTLV-1 is known to infect many types of cells in vivo (31), the majority of HTLV-1-infected cells are $CD4^+$ memory T cells (46, 62). To determine the effect of HTLV-1 infection on subpopulations of lymphocytes, we studied the expression of surface molecules by flow cytometry. Two weeks after infection, there was a significant increase in the cell population expressing CD4 and CD45RO molecules in the infected group compared to that in the control group (Fig. 1), suggesting that in the infected group of mice, memory $CD4^+$ T cells proliferated. This finding is consistent with observations with HTLV-1 carriers (62). The proviral loads in $CD4^+$ and $CD8^+$ splenic T cells were determined by real-time PCR (Table 4). As previously reported for HTLV-1 carriers, $CD8^+$ T cells were also found to contain the provirus, but to a lesser extent than $CD4^+$ T cells (39, 62). Nevertheless, proviral load tended to increase with time in both subpopulations of T cells (Table 4).

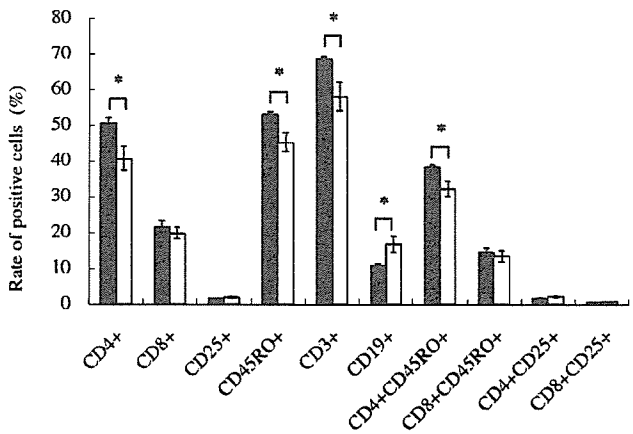

FIG. 1. Surface marker analysis of splenocytes in hu-PBMC-NOG mice. Splenocytes were isolated from hu-PBMC-NOG mice with or without HTLV-1 infection, and their surface markers were analyzed by flow cytometry. Splenocytes were recovered at 2 weeks p.i. The percentages of cells positive for various surface molecules are shown for MT-2-inoculated hu-PBMC-NOG mice (black bars) and uninfected controls (open bars). Values are means ± standard deviations from groups of three mice. *, $P < 0.05$ (Student's t test).

Polyclonal proliferation of HTLV-1-infected cells. In HTLV-1 carriers, polyclonal proliferation of HTLV-1 infected cells has been detected (10). Therefore, the clonality of HTLV-1-infected cells in hu-PBMC-NOG mice was analyzed by IL-PCR. We analyzed the same DNA samples in triplicate. When the same bands are detected in all three reactions, it means that the number of such clones is high. On the other hand, the stochastic results suggest that these clones are minor in vivo. As shown in Fig. 2, multiple bands were detected by IL-PCR at the 2-week time point, indicating an early polyclonal proliferation. At the 4-week time point, the number of bands increased, as did the intensity of bands corresponding to major clones, suggesting that both the numbers of clones and cell numbers of major clones increased (Fig. 2). We further confirmed the presence of different clones in the same mouse by determining the integration sites of the provirus in the human cells (data not shown).

Profile of proviral DNA methylation in primary HTLV-1 infection. Proviral DNA methylation appears to begin at the internal sequences, such as the *gag*, *pol*, and *env* regions (54), and accumulates in vivo. DNA methylation is thought to disturb viral gene transcription when the 5′ long terminal repeat (LTR) is methylated by inhibiting the binding of transcriptional factors (6). We analyzed the DNA methylation status of the proviral DNA in the cells recovered from the mice (Fig. 3). In the 2-week group, none of the three samples tested presented methylation in the *gag*, *pol*, or 5′ LTR regions. However, in the cells recovered from two mice after 4 weeks, the *gag* regions from both mice were partially methylated, and the *pol* region from one of the two mice was methylated. These results coincide with our previous findings that CpG motifs within the proviral sequence of HTLV-1 are methylated in a progressive manner, starting from internal regions and then spreading to the 5′ and 3′ ends of the provirus (54).

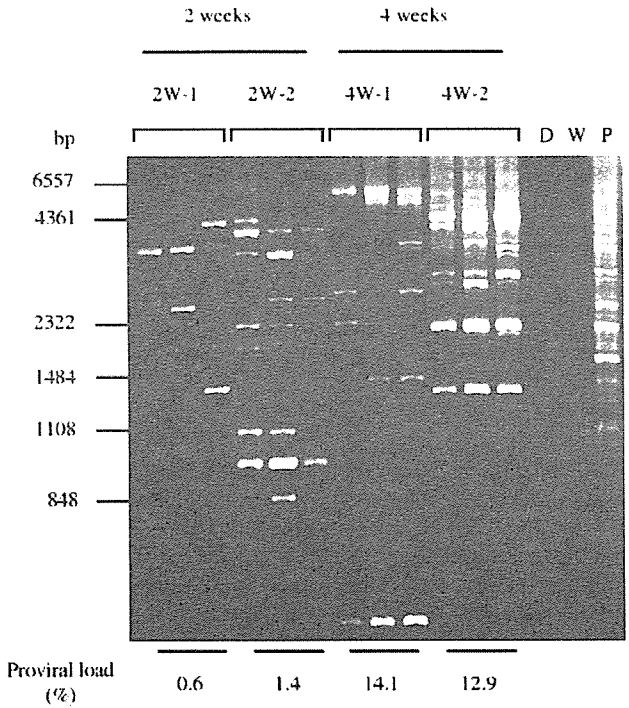

FIG. 2. Polyclonal proliferation of HTLV-1-infected cells in the spleens of hu-PBMC-NOG mice (2W-1, 2W-2, 4W-1, and 4W-2). Genomic DNA was isolated from recovered splenocytes and analyzed by IL-PCR as described in Materials and Methods. IL-PCR was performed in triplicate for each DNA sample. Genomic DNA was recovered from splenocytes at 2 or 4 weeks after injection of MT-2 cells. D, DNA of donor PBMC before inoculation; W, water; P, positive control (DNA from PBMC of an HTLV-1 carrier). In addition, proviral load was quantified by real-time PCR as described in Materials and Methods and is shown as a relative percentage.

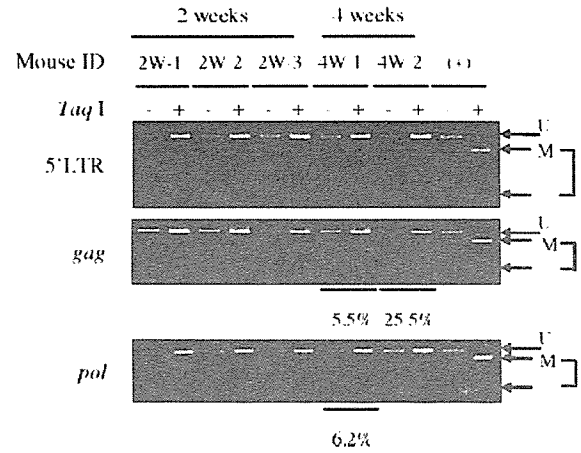

FIG. 3. DNA methylation of HTLV-1 provirus. hu-PBMC-NOG mice were sacrificed 2 or 4 weeks after inoculation of MT-2 cells, and DNA methylation in the 5′ LTR, *gag*, and *pol* regions was studied by a COBRA assay. (+), positive control; U, intact fragment (unmethylated CpG); M, digested fragments (methylated CpG). Percentages of DNA methylation were calculated by densitography according to the following formula (with the variables as described above): [M/(U + M)] × 100.

Suppression of *tax* gene transcription in the NOG mouse model. The viral protein Tax is believed to play an important role in the proliferation of infected cells due to its pleiotropic functions (63). However, its expression in vivo has not been detected in most ATL patients (52). When ATL cells are transferred to culture ex vivo, Tax expression can be recovered (21, 30, 57). Viral gene transcription is also suppressed in PBMC of HAM/TSP patients, as well as asymptomatic HTLV-1 carriers (19, 28). We performed an RT-PCR in order to detect *tax* mRNA in the spleens of infected hu-PBMC-NOG mice sacrificed 2 weeks p.i. (Fig. 4). Transcripts of the *tax* gene were undetectable in two of the three mice when cells were recovered, while the remaining one showed a low level of expression. In all three cases, there was an increase of *tax* gene transcription after 24 h of culture in vitro, even without changes in the proviral load (Fig. 4). Since this phenomenon occurs even in hu-PBMC-NOG mice, a factor(s) other than the host immune system must be involved in the suppression of *tax* gene transcription in vivo.

Effect of antiretroviral agents on HTLV-1 infection. It is well known that HTLV-1 is transmitted through sexual intercourse (49), breast feeding (48), and blood transfusions (42), and for transmission, cell-to-cell contact is thought to be essential. Due to the low capacity of cell-free virus to infect (8, 11), accidental exposures were not thought to confer a high risk of infection, and no prophylactic therapy has been considered. However, the prevalence of HTLV-1 carriers among drug abusers shows that we do need to develop strategies to prevent viral transmission. A previous in vitro study reported that AZT was able to inhibit new HTLV-1 infection of human lymphocytes (37). In addition, it has been reported that tenofovir efficiently inhibited the reverse transcriptase activity of HTLV-1 (20). In order to assess whether a preventive antiretroviral treatment would prove useful in cases of accidental HTLV-1 exposure, we treated hu-PBMC-NOG mice with two reverse transcriptase inhibitors, AZT and tenofovir. The treatment started as soon as MT-2 cells were injected and continued for 12 days. Proviral DNA was undetectable by real-time PCR in the groups of mice treated with AZT or tenofovir (Table 5). Mice seemed to tolerate the treatment without evident signs of toxicity. In the cases where weight loss was seen, it did not exceed 6% of the weight at the time treatment was started (data not shown). However, the number of human cells recovered from spleens of mice receiving AZT treatment was lower than those of the other two groups (Table 5), which indicates that this drug might be also interfering in the proliferation of transferred PBMC. In in vitro assays, we analyzed the cytotoxic effects of AZT and tenofovir on PHA-stimulated human PBMC derived from three different donors. We found that, in a range of concentrations from 5 mM to 0.05 μM, AZT was more toxic than tenofovir when used in incubations for 3 days (Fig. 5). The 50% cytotoxic concentration of AZT was 0.297 ± 0.169 mM, while that of tenofovir was higher than 5 mM. These results indicate that the cytotoxic effect of AZT contributes to suppression of the number of transferred human lymphocytes in our mouse in addition to inhibition of reverse transcriptase.

Clonal expansion of infected cells takes place even in the early stages of primary HTLV-1 infection. It remains undeter-

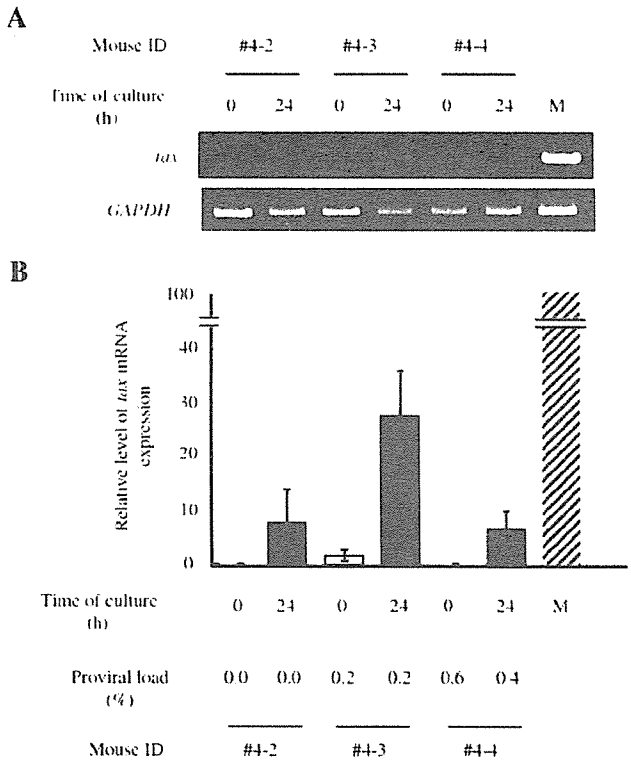

FIG. 4. Transcription of the *tax* gene increases after in vitro culture. Splenocytes of hu-PBMC-NOG mice inoculated with 10^4 MT-2 cells were recovered 2 weeks after infection. Transcription of the *tax* gene was quantified by semiquantitative PCR (A) or real-time PCR (B) at recovery and after 24 h of in vitro culture. Proviral loads for the same samples were also measured by real-time PCR. M, MT-1 cells; ID, identification number.

mined whether clonal proliferation or internal continuous contagion contributes to the increase of HTLV-1-infected cells. To answer this question, hu-PBMC-NOG mice infected with MT-2 cells were treated with tenofovir beginning 1 week after infection. Tenofovir treatment made no significant difference in HTLV-1 proviral load (Table 6), suggesting that clonal proliferation is predominant after HTLV-1 infection. The provirus loads of AZT-treated mice were lower than those of untreated mice, suggesting that the cytotoxic effect of AZT suppressed the provirus loads, as shown in Table 6.

DISCUSSION

Human immunodeficiency virus type 1 vigorously generates progeny virions through the action of its accessory genes, and the resulting free virions play an important role in its transmission, in addition to cell-to-cell transmission. In contrast, for HTLV-1, the efficiency of transmission by free virions is much lower than that via cell-to-cell contact (8), suggesting that HTLV-1 transmits primarily through the latter mechanism. To facilitate such transmission, instead of producing virions, HTLV-1 increases the number of infected cells by the actions of its accessory genes (17, 63). The finding that mother-to-infant transmission was more frequent in mothers with higher proviral loads indicates that such an increase in the number of

TABLE 5. RT inhibitors AZT and tenofovir inhibit de novo infection by HTLV-1[a]

Condition or treatment	Mouse	Proviral load (%)		Cell count (10^6)
		Lavage specimen	Spleen	
Untreated	C1	4.2	1.1	1.6
	C2	0.7	0.0	12.5
	C3	0.0	0.0	19.0
	C4	5.9	0.6	6.0
	C5	0.1	0.1	4.8
Tenofovir	T1	0.0	0.0	5.2
	T2	0.0	0.0	9.2
	T3	0.0	0.0	1.7
	T4	0.0	0.0	8.8
	T5	0.0	0.0	4.0
AZT	A1	0.0	0.0	2.6
	A2	0.0	0.0	3.6
	A3	0.0	0.0	4.5
	A4	0.0	0.0	2.2
	A5	0.0	0.0	2.3

[a] After human PBMC transfer and MT-2 inoculation (10^3 cells/mouse), mice were immediately subjected to antiretroviral therapy with AZT or tenofovir for 12 days. The control group was injected with PBS instead. Proviral loads were determined in cells recovered from the abdominal cavity and spleens. The total numbers of cells recovered from spleens are also shown.

infected cells facilitates the transmission of HTLV-1 (33). In vivo studies using animal models show that the early stage of HTLV-1 infection is controlled by accessory genes, including *p12*, *p13*, *p30*, and *HBZ* genes (3, 5, 22, 47). Thus, although in vivo studies using animal models revealed the importance of accessory genes in replication of HTLV-1 and proliferation of infected cells, the events in the early stages of in vivo transmission in human lymphocytes have not been studied yet due to the lack of an appropriate animal model. Since the metabolisms of nucleosides are quite different among animal species, it is critical to study the effect of reverse transcriptase inhibitors on HTLV-1 in human lymphocytes.

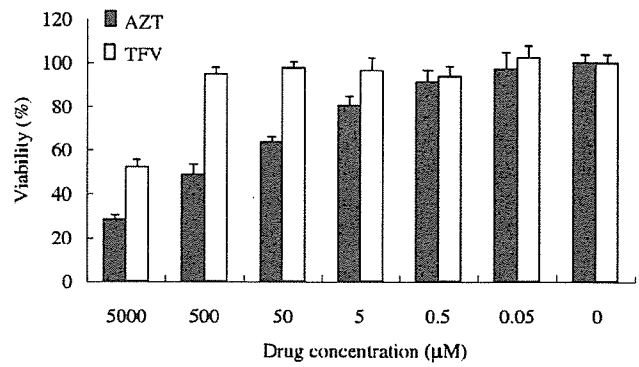

FIG. 5. Cytotoxic effects of tenofovir (TFV) and AZT in vitro. Human PBMC were stimulated with PHA for 3 days. Cells were then cultured in medium alone or medium containing the specified concentration of the indicated drug for another three days, at a density of 10^5 cells/well, in a 96-well plate. Viability was assessed by MTT assay as described in Materials and Methods. The results show the means ± standard deviations of quadruplicate measurements made in one of three representative experiments.

TABLE 6. Proviral load after treatment with tenofovir or AZT beginning one week after infection[a]

Condition or treatment	Mouse	Proviral load (%)	
		Lavage specimen	Spleen
Untreated	U11	7.4	1.7
	U12	0.1	0.0
	U13	15.4	1.9
	U14	3.8	0.7
Tenofovir	T11	0.0	0.0
	T12	0.2	0.0
	T13	15.9	1.8
	T14	14.5	2.6
Untreated	U21	0.6	0.1
	U22	ND	3.0
	U23	12.6	1.0
	U24	11.6	0.8
AZT	A21	0.0	0.0
	A22	ND	0.6
	A23	2.5	0.0
	A24	0.1	0.0

[a] After human PBMC transfer and MT-2 inoculation (10^3 cells/mouse for the tenofovir group, and 10^4 cells/mouse for the AZT group), mice were left for one week before starting treatment with tenofovir or AZT. The control groups were injected with PBS instead of the drugs. Mice were sacrificed 7 or 12 days after treatment with AZT or tenofovir, respectively. Splenocytes, as well as cells from the abdominal cavity, were recovered for analysis as described in Materials and Methods. ND, not determined.

It is widely accepted that the HTLV-1 virion per se is poorly infectious (8, 11) and that cell-to-cell transmission is more efficient both in vivo and in vitro (23, 42, 45, 61). Among drug abusers, HTLV-1 infection has been reported, indicating that HTLV-1 can be transmitted by the sharing of needles (12). Therefore, in cases of accidental exposure to HTLV-1-positive blood, preventive administration of antiretroviral drugs should be considered. In this study, we proved that the administration of a reverse transcriptase inhibitor beginning immediately after exposure can block HTLV-1 transmission. However, a delay in its administration may render it ineffective at preventing HTLV-1 transmission due to the importance of clonal expansion in the biology of this virus.

In particular, whether clonal expansion or internal continuous contagion is important in increasing the number of infected cells still remains unknown. A previous study reported that a reverse transcriptase inhibitor, lamivudine, reduced the proviral load in a patient with HAM/TSP (56), implicating internal contagion in maintaining the number of infected cells in vivo. However, another study reported that lamivudine had no definite effect on proviral load (34). In this study, administering tenofovir to block the spread of infection to new cells did not influence the proviral load in hu-PBMC-NOG mice, even though tenofovir has been reported to be more efficient in inhibiting HTLV-1 replication than lamivudine (20). Taken together, these results suggest that clonal proliferation contributes to the increase of HTLV-1-infected cells more than internal contagion even early in HTLV-1 infection. Recently, one study reported that clonality of HTLV-1-infected cells was variable after seroconversion but it became stable over time, indicating that the host immune system selected certain HTLV-1-infected clones (53). Since there is little or no host immune response to HTLV-1-infected cells in our system, it is possible that clonal proliferation of HTLV-1-infected cells is influenced by their ability to produce HTLV-1-encoded proteins, such as Tax. The factors including integration of the provirus in certain sites of the genome might also contribute to the variable proliferation of infected cells.

Viral gene transcription in HTLV-1-infected cells and ATL cells is suppressed in vivo. However, when they are cultured in vitro, transcription is rapidly recovered (54). Regarding the mechanisms of in vivo suppression, one possibility is that CTLs kill Tax-expressing cells, and the other is that nonimmune factors suppress it. The removal of $CD8^+$ T lymphocytes from PBMC derived from seropositive carriers enhanced Tax expression, suggesting that CTLs were indeed involved in inhibiting Tax expression in vivo (15, 18). On the other hand, a nonimmune factor(s) might be involved in this suppression. In this study, we showed that *tax* gene transcription was enhanced after in vitro culture. This finding is very similar to the phenomenon in carriers. It is noteworthy that in our system, there is no immune response to HTLV-1, indicating that a nonimmune factor(s) suppresses *tax* gene expression in vivo. These results suggest that both immune and nonimmune factors may be involved in the silencing of *tax* gene transcription.

Methylation of proviral DNA is regarded as a kind of host defense mechanism to suppress viral gene expression. However, HTLV-1 utilizes this epigenetic modification to escape the host immune surveillance. In cells immortalized by HTLV-1 in vitro, there was little DNA methylation in the provirus. In humans, on the other hand, DNA methylation accumulated within one year after seroconversion (54). In our system, DNA methylation was detected in the *pol* and *gag* regions 4 weeks after inoculation of MT-2 cells, indicating that HTLV-1 provirus is prone to methylation in vivo. Since *tax* gene transcription is silenced in hu-PBMC-NOG mice as shown in this study, such suppression might promote DNA methylation in vivo. On the other hand, since proliferation of HTLV-1-immortalized T lymphocytes is likely dependent on Tax expression, we speculate that cells with unmethylated provirus have growth advantages. We previously reported that histone H3 was hyperacetylated in the 5′ LTR of ATL cells without *tax* gene transcription, and such ATL cells transcribed *tax* gene within one hour after in vitro culture (54). This suggests the presence of a factor(s) inhibitory to *tax* gene transcription whose inhibition is nullified in in vitro culture. Such a mechanism, with the capacity for quickly switching on and off, would be useful for controlling *tax* gene transcription in vivo and thus enabling HTLV-1-infected cells to escape the host immune response.

In this study, we established an in vivo system for de novo infection with HTLV-1 and observed that the phenotype of HTLV-1-infected cells resembled that in the carrier state. The limitation of this in vivo system is that the long-term persistence of de novo infection in hu-PBMC-NOG mice cannot be examined, due to the graft-versus-host disease caused by implanted human lymphocytes. On the other hand, its merit is that the severe immune deficiency of this strain allows the vigorous proliferation of human lymphocytes, previously reported to be the result of a hyperactivation of the cells (40),

which enables HTLV-1 to rapidly spread by cell-to-cell contact. Therefore, this model system should be a useful tool for analyzing the events in the early stage of HTLV-1 infection in human lymphocytes.

ACKNOWLEDGMENTS

We thank Gilead Sciences Inc. for generously providing tenofovir for this study and Linda Kingsbury for excellent proofreading.

This study was supported by a grant-in-aid for scientific research from the Ministry of Education, Science, Sports, and Culture of Japan.

REFERENCES

1. **Akagi, T., I. Takeda, T. Oka, Y. Ohtsuki, S. Yano, and I. Miyoshi.** 1985. Experimental infection of rabbits with human T-cell leukemia virus type I. Jpn. J. Cancer Res. **76**:86–94.
2. **Albrecht, B., C. D. D'Souza, W. Ding, S. Tridandapani, K. M. Coggeshall, and M. D. Lairmore.** 2002. Activation of nuclear factor of activated T cells by human T-lymphotropic virus type 1 accessory protein $p12^{I}$. J. Virol. **76**:3493–3501.
3. **Arnold, J., B. Yamamoto, M. Li, A. J. Phipps, I. Younis, M. D. Lairmore, and P. L. Green.** 2006. Enhancement of infectivity and persistence in vivo by HBZ, a natural antisense coded protein of HTLV-1. Blood **107**:3976–3982.
4. **Bangham, C. R., and M. Osame.** 2005. Cellular immune response to HTLV-1. Oncogene **24**:6035–6046.
5. **Collins, N. D., G. C. Newbound, B. Albrecht, J. L. Beard, L. Ratner, and M. D. Lairmore.** 1998. Selective ablation of human T-cell lymphotropic virus type 1 p12I reduces viral infectivity in vivo. Blood **91**:4701–4707.
6. **Datta, S., N. H. Kothari, and H. Fan.** 2000. In vivo genomic footprinting of the human T-cell leukemia virus type 1 (HTLV-1) long terminal repeat enhancer sequences in HTLV-1-infected human T-cell lines with different levels of Tax I activity. J. Virol. **74**:8277–8285.
7. **Debacq, C., J. M. Heraud, B. Asquith, C. Bangham, F. Merien, V. Moules, F. Mortreux, E. Wattel, A. Burny, R. Kettmann, M. Kazanji, and L. Willems.** 2005. Reduced cell turnover in lymphocytic monkeys infected by human T-lymphotropic virus type 1. Oncogene **24**:7514–7523.
8. **Derse, D., S. A. Hill, P. A. Lloyd, H. Chung, and B. A. Morse.** 2001. Examining human T-lymphotropic virus type 1 infection and replication by cell-free infection with recombinant virus vectors. J. Virol. **75**:8461–8468.
9. **Dewan, M. Z., K. Terashima, M. Taruishi, H. Hasegawa, M. Ito, Y. Tanaka, N. Mori, T. Sata, Y. Koyanagi, M. Maeda, Y. Kubuki, A. Okayama, M. Fujii, and N. Yamamoto.** 2003. Rapid tumor formation of human T-cell leukemia virus type 1-infected cell lines in novel NOD-SCID/γc^{null} mice: suppression by an inhibitor against NF-κB. J. Virol. **77**:5286–5294.
10. **Etoh, K., S. Tamiya, K. Yamaguchi, A. Okayama, H. Tsubouchi, T. Ideta, N. Mueller, K. Takatsuki, and M. Matsuoka.** 1997. Persistent clonal proliferation of human T-lymphotropic virus type I-infected cells in vivo. Cancer Res. **57**:4862–4867.
11. **Fan, N., J. Gavalchin, B. Paul, K. H. Wells, M. J. Lane, and B. J. Poiesz.** 1992. Infection of peripheral blood mononuclear cells and cell lines by cell-free human T-cell lymphoma/leukemia virus type I. J. Clin. Microbiol. **30**:905–910.
12. **Feigal, E., E. Murphy, K. Vranizan, P. Bacchetti, R. Chaisson, J. E. Drummond, W. Blattner, M. McGrath, J. Greenspan, and A. Moss.** 1991. Human T cell lymphotropic virus types I and II in intravenous drug users in San Francisco: risk factors associated with seropositivity. J. Infect. Dis. **164**:36–42.
13. **Feuer, G., J. A. Zack, W. J. Harrington, Jr., R. Valderama, J. D. Rosenblatt, W. Wachsman, S. M. Baird, and I. S. Chen.** 1993. Establishment of human T-cell leukemia virus type I T-cell lymphomas in severe combined immunodeficient mice. Blood **82**:722–731.
14. **Franchini, G., R. Fukumoto, and J. R. Fullen.** 2003. T-cell control by human T-cell leukemia/lymphoma virus type 1. Int. J. Hematol. **78**:280–296.
15. **Furuta, R. A., K. Sugiura, S. Kawakita, T. Inada, S. Ikehara, T. Matsuda, and J. Fujisawa.** 2002. Mouse model for the equilibration interaction between the host immune system and human T-cell leukemia virus type 1 gene expression. J. Virol. **76**:2703–2713.
16. **Gessain, A., F. Barin, J. C. Vernant, O. Gout, L. Maurs, A. Calender, and G. de The.** 1985. Antibodies to human T-lymphotropic virus type-I in patients with tropical spastic paraparesis. Lancet **ii**:407–410.
17. **Grassmann, R., M. Aboud, and K. T. Jeang.** 2005. Molecular mechanisms of cellular transformation by HTLV-1 Tax. Oncogene **24**:5976–5985.
18. **Hanon, E., S. Hall, G. P. Taylor, M. Saito, R. Davis, Y. Tanaka, K. Usuku, M. Osame, J. N. Weber, and C. R. Bangham.** 2000. Abundant tax protein expression in CD4+ T cells infected with human T-cell lymphotropic virus type I (HTLV-I) is prevented by cytotoxic T lymphocytes. Blood **95**:1386–1392.
19. **Hanon, E., J. C. Stinchcombe, M. Saito, B. E. Asquith, G. P. Taylor, Y. Tanaka, J. N. Weber, G. M. Griffiths, and C. R. Bangham.** 2000. Fratricide among CD8(+) T lymphocytes naturally infected with human T cell lymphotropic virus type I. Immunity **13**:657–664.
20. **Hill, S. A., P. A. Lloyd, S. McDonald, J. Wykoff, and D. Derse.** 2003. Susceptibility of human T cell leukemia virus type I to nucleoside reverse transcriptase inhibitors. J. Infect. Dis. **188**:424–427.
21. **Hinuma, Y., Y. Gotoh, K. Sugamura, K. Nagata, T. Goto, M. Nakai, N. Kamada, T. Matsumoto, and K. Kinoshita.** 1982. A retrovirus associated with human adult T-cell leukemia: in vitro activation. Gann **73**:341–344.
22. **Hiraragi, H., S. J. Kim, A. J. Phipps, M. Silic-Benussi, V. Ciminale, L. Ratner, P. L. Green, and M. D. Lairmore.** 2006. Human T-lymphotropic virus type 1 mitochondrion-localizing protein $p13^{II}$ is required for viral infectivity in vivo. J. Virol. **80**:3469–3476.
23. **Igakura, T., J. C. Stinchcombe, P. K. Goon, G. P. Taylor, J. N. Weber, G. M. Griffiths, Y. Tanaka, M. Osame, and C. R. Bangham.** 2003. Spread of HTLV-I between lymphocytes by virus-induced polarization of the cytoskeleton. Science **299**:1713–1716.
24. **Imada, K., A. Takaori-Kondo, T. Akagi, K. Shimotohno, K. Sugamura, T. Hattori, H. Yamabe, M. Okuma, and T. Uchiyama.** 1995. Tumorigenicity of human T-cell leukemia virus type I-infected cell lines in severe combined immunodeficient mice and characterization of the cells proliferating in vivo. Blood **86**:2350–2357.
25. **Ito, M., H. Hiramatsu, K. Kobayashi, K. Suzue, M. Kawahata, K. Hioki, Y. Ueyama, Y. Koyanagi, K. Sugamura, K. Tsuji, T. Heike, and T. Nakahata.** 2002. NOD/SCID/gamma(c) (null) mouse: an excellent recipient mouse model for engraftment of human cells. Blood **100**:3175–3182.
26. **Johnson, J. M., C. Nicot, J. Fullen, V. Ciminale, L. Casareto, J. C. Mulloy, S. Jacobson, and G. Franchini.** 2001. Free major histocompatibility complex class I heavy chain is preferentially targeted for degradation by human T-cell leukemia/lymphotropic virus type 1 $p12^{I}$ protein. J. Virol. **75**:6086–6094.
27. **Kannagi, M., S. Harada, I. Maruyama, H. Inoko, H. Igarashi, G. Kuwashima, S. Sato, M. Morita, M. Kidokoro, M. Sugimoto, et al.** 1991. Predominant recognition of human T cell leukemia virus type I (HTLV-I) pX gene products by human CD8+ cytotoxic T cells directed against HTLV-I-infected cells. Int. Immunol. **3**:761–767.
28. **Kannagi, M., S. Matsushita, H. Shida, and S. Harada.** 1994. Cytotoxic T cell response and expression of the target antigen in HTLV-I infection. Leukemia **8**(Suppl. 1):S54–S59.
29. **Kim, S. J., A. M. Nair, S. Fernandez, L. Mathes, and M. D. Lairmore.** 2006. Enhancement of LFA-1-mediated T cell adhesion by human T lymphotropic virus type 1 p12I1. J. Immunol. **176**:5463–5470.
30. **Kinoshita, T., M. Shimoyama, K. Tobinai, M. Ito, S. Ito, S. Ikeda, K. Tajima, K. Shimotohno, and T. Sugimura.** 1989. Detection of mRNA for the tax1/rex1 gene of human T-cell leukemia virus type I in fresh peripheral blood mononuclear cells of adult T-cell leukemia patients and viral carriers by using the polymerase chain reaction. Proc. Natl. Acad. Sci. USA **86**:5620–5624.
31. **Koyanagi, Y., Y. Itoyama, N. Nakamura, K. Takamatsu, J. Kira, T. Iwamasa, I. Goto, and N. Yamamoto.** 1993. In vivo infection of human T-cell leukemia virus type I in non-T cells. Virology **196**:25–33.
32. **Lairmore, M. D., L. Silverman, and L. Ratner.** 2005. Animal models for human T-lymphotropic virus type 1 (HTLV-1) infection and transformation. Oncogene **24**:6005–6015.
33. **Li, H. C., R. J. Biggar, W. J. Miley, E. M. Maloney, B. Cranston, B. Hanchard, and M. Hisada.** 2004. Provirus load in breast milk and risk of mother-to-child transmission of human T lymphotropic virus type I. J. Infect. Dis. **190**:1275–1278.
34. **Machuca, A., B. Rodes, and V. Soriano.** 2001. The effect of antiretroviral therapy on HTLV infection. Virus Res. **78**:93–100.
35. **Manel, N., F. J. Kim, S. Kinet, N. Taylor, M. Sitbon, and J. L. Battini.** 2003. The ubiquitous glucose transporter GLUT-1 is a receptor for HTLV. Cell **115**:449–459.
36. **Matsuoka, M., and K. T. Jeang.** 2005. Human T-cell leukemia virus type I at age 25: a progress report. Cancer Res. **65**:4467–4470.
37. **Matsushita, S., H. Mitsuya, M. S. Reitz, and S. Broder.** 1987. Pharmacological inhibition of in vitro infectivity of human T lymphotropic virus type I. J. Clin. Investig. **80**:394–400.
38. **Michael, B., A. M. Nair, H. Hiraragi, L. Shen, G. Feuer, K. Boris-Lawrie, and M. D. Lairmore.** 2004. Human T lymphotropic virus type-1 p30II alters cellular gene expression to selectively enhance signaling pathways that activate T lymphocytes. Retrovirology **1**:39.
39. **Nagai, M., M. B. Brennan, J. A. Sakai, C. A. Mora, and S. Jacobson.** 2001. CD8(+) T cells are an in vivo reservoir for human T-cell lymphotropic virus type I. Blood **98**:1858–1861.
40. **Nakata, H., K. Maeda, T. Miyakawa, S. Shibayama, M. Matsuo, Y. Takaoka, M. Ito, Y. Koyanagi, and H. Mitsuya.** 2005. Potent anti-R5 human immunodeficiency virus type 1 effects of a CCR5 antagonist, AK602/ONO4128/GW873140, in a novel human peripheral blood mononuclear cell nonobese diabetic-SCID, interleukin-2 receptor gamma-chain-knocked-out AIDS mouse model. J. Virol. **79**:2087–2096.
41. **Nicot, C., M. Dundr, J. M. Johnson, J. R. Fullen, N. Alonzo, R. Fukumoto, G. L. Princler, D. Derse, T. Misteli, and G. Franchini.** 2004. HTLV-1-

encoded p30II is a post-transcriptional negative regulator of viral replication. Nat. Med. **10**:197–201.
42. **Okochi, K., and H. Sato.** 1984. Transmission of ATLV (HTLV-I) through blood transfusion. Princess Takamatsu Symp. **15**:129–135.
43. **Osame, M., K. Usuku, S. Izumo, N. Ijichi, H. Amitani, A. Igata, M. Matsumoto, and M. Tara.** 1986. HTLV-I associated myelopathy, a new clinical entity. Lancet **i**:1031–1032.
44. **Poiesz, B. J., F. W. Ruscetti, A. F. Gazdar, P. A. Bunn, J. D. Minna, and R. C. Gallo.** 1980. Detection and isolation of type C retrovirus particles from fresh and cultured lymphocytes of a patient with cutaneous T-cell lymphoma. Proc. Natl. Acad. Sci. USA **77**:7415–7419.
45. **Popovic, M., P. S. Sarin, M. Robert-Gurroff, V. S. Kalyanaraman, D. Mann, J. Minowada, and R. C. Gallo.** 1983. Isolation and transmission of human retrovirus (human T-cell leukemia virus). Science **219**:856–859.
46. **Richardson, J. H., A. J. Edwards, J. K. Cruickshank, P. Rudge, and A. G. Dalgleish.** 1990. In vivo cellular tropism of human T-cell leukemia virus type 1. J. Virol. **64**:5682–5687.
47. **Silverman, L. R., A. J. Phipps, A. Montgomery, L. Ratner, and M. D. Lairmore.** 2004. Human T-cell lymphotropic virus type 1 open reading frame II-encoded $p30^{II}$ is required for in vivo replication: evidence of in vivo reversion. J. Virol. **78**:3837–3845.
48. **Sugiyama, H., H. Doi, K. Yamaguchi, Y. Tsuji, T. Miyamoto, and S. Hino.** 1986. Significance of postnatal mother-to-child transmission of human T-lymphotropic virus type-I on the development of adult T-cell leukemia/lymphoma. J. Med. Virol. **20**:253–260.
49. **Tajima, K., S. Tominaga, and T. Suchi.** 1986. Malignant lymphomas in Japan: epidemiological analysis on adult T-cell leukemia/lymphoma. Hematol. Oncol. **4**:31–44.
50. **Takatsuki, K.** 2005. Discovery of adult T-cell leukemia. Retrovirology **2**:16.
51. **Takatsuki, K., T. Uchiyama, K. Sagawa, and J. Yodoi.** 1977. Adult T cell leukemia in Japan, p. 73–77. *In* S. Seno, F. Takaku, and S. Irino (ed.), Topic in hematology. The 16th International Congress of Hematology. Excerpta Medica, Amsterdam, The Netherlands.
52. **Takeda, S., M. Maeda, S. Morikawa, Y. Taniguchi, J. Yasunaga, K. Nosaka, Y. Tanaka, and M. Matsuoka.** 2004. Genetic and epigenetic inactivation of tax gene in adult T-cell leukemia cells. Int. J. Cancer **109**:559–567.
53. **Tanaka, G., A. Okayama, T. Watanabe, S. Aizawa, S. Stuver, N. Mueller, C. C. Hsieh, and H. Tsubouchi.** 2005. The clonal expansion of human T lymphotropic virus type 1-infected T cells: a comparison between seroconverters and long-term carriers. J. Infect. Dis. **191**:1140–1147.
54. **Taniguchi, Y., K. Nosaka, J. Yasunaga, M. Maeda, N. Mueller, A. Okayama, and M. Matsuoka.** 2005. Silencing of human T-cell leukemia virus type I gene transcription by epigenetic mechanisms. Retrovirology **2**:64.
55. **Tateno, M., N. Kondo, T. Itoh, T. Chubachi, T. Togashi, and T. Yoshiki.** 1984. Rat lymphoid cell lines with human T cell leukemia virus production. I. Biological and serological characterization. J. Exp. Med. **159**:1105–1116.
56. **Taylor, G. P., S. E. Hall, S. Navarrete, C. A. Michie, R. Davis, A. D. Witkover, M. Rossor, M. A. Nowak, P. Rudge, E. Matutes, C. R. Bangham, and J. N. Weber.** 1999. Effect of lamivudine on human T-cell leukemia virus type 1 (HTLV-1) DNA copy number, T-cell phenotype, and anti-Tax cytotoxic T-cell frequency in patients with HTLV-1-associated myelopathy. J. Virol. **73**:10289–10295.
57. **Uchiyama, T.** 1997. Human T cell leukemia virus type I (HTLV-I) and human diseases. Annu. Rev. Immunol. **15**:15–37.
58. **Uchiyama, T., J. Yodoi, K. Sagawa, K. Takatsuki, and H. Uchino.** 1977. Adult T-cell leukemia: clinical and hematologic features of 16 cases. Blood **50**:481–492.
59. **Xiong, Z., and P. W. Laird.** 1997. COBRA: a sensitive and quantitative DNA methylation assay. Nucleic Acids Res. **25**:2532–2534.
60. **Yahata, T., K. Ando, Y. Nakamura, Y. Ueyama, K. Shimamura, N. Tamaoki, S. Kato, and T. Hotta.** 2002. Functional human T lymphocyte development from cord blood CD34+ cells in nonobese diabetic/Shi-scid, IL-2 receptor gamma null mice. J. Immunol. **169**:204–209.
61. **Yamamoto, N., M. Okada, Y. Koyanagi, M. Kannagi, and Y. Hinuma.** 1982. Transformation of human leukocytes by cocultivation with an adult T cell leukemia virus producer cell line. Science **217**:737–739.
62. **Yasunaga, J., T. Sakai, K. Nosaka, K. Etoh, S. Tamiya, S. Koga, S. Mita, M. Uchino, H. Mitsuya, and M. Matsuoka.** 2001. Impaired production of naive T lymphocytes in human T-cell leukemia virus type I-infected individuals: its implications in the immunodeficient state. Blood **97**:3177–3183.
63. **Yoshida, M.** 2001. Multiple viral strategies of HTLV-1 for dysregulation of cell growth control. Annu. Rev. Immunol. **19**:475–496.
64. **Zhang, W., J. W. Nisbet, B. Albrecht, W. Ding, F. Kashanchi, J. T. Bartoe, and M. D. Lairmore.** 2001. Human T-lymphotropic virus type 1 $p30^{II}$ regulates gene transcription by binding CREB binding protein/p300. J. Virol. **75**:9885–9895.
65. **Zhao, T. M., B. Hague, D. L. Caudell, R. M. Simpson, and T. J. Kindt.** 2005. Quantification of HTLV-I proviral load in experimentally infected rabbits. Retrovirology **2**:34.

Antiviral Chemistry & Chemotherapy 17:167–174

Rapid propagation of low-fitness drug-resistant mutants of human immunodeficiency virus type 1 by a streptococcal metabolite sparsomycin

Kosuke Miyauchi, Jun Komano*, Lay Myint, Yuko Futahashi, Emiko Urano, Zene Matsuda, Tomoko Chiba, Hideka Miura, Wataru Sugiura and Naoki Yamamoto

AIDS Research Center, National Institute of Infectious Diseases, Toyama, Shinjuku, Tokyo, Japan

*Corresponding author: Tel: +81 3 5285 1111; Fax: +81 3 5285 5037; E-mail: ajkomano@nih.go.jp

Here we report that sparsomycin, a streptococcal metabolite, enhances the replication of HIV-1 in multiple human T cell lines at a concentration of 400 nM. In addition to wild-type HIV-1, sparsomycin also accelerated the replication of low-fitness, drug-resistant mutants carrying either D30N or L90M within HIV-1 protease, which are frequently found mutations in HIV-1-infected patients on highly active antiretroviral therapy (HAART). Of particular interest was that replication enhancement appeared profound when HIV-1 such as the L90M-carrying mutant displayed relatively slower replication kinetics. The presence of sparsomycin did not immediately select the fast-replicating HIV-1 mutants in culture. In addition, sparsomycin did not alter the 50% inhibitory concentration (IC_{50}) of antiretroviral drugs directed against HIV-1 including nucleoside reverse transcriptase inhibitors (lamivudine and stavudine), non-nucleoside reverse transcriptase inhibitor (nevirapine) and protease inhibitors (nelfinavir, amprenavir and indinavir). The IC_{50}s of both zidovudine and lopinavir against multidrug resistant HIV-1 in the presence of sparsomycin were similar to those in the absence of sparsomycin. The frameshift reporter assay and Western blot analysis revealed that the replication-boosting effect was partly due to the sparsomycin's ability to increase the –1 frameshift efficiency required to produce the *Gag–Pol* transcript. In conclusion, the use of sparsomycin should be able to facilitate the drug resistance profiling of the clinical isolates and the study on the low-fitness viruses.

Keywords: drug resistant mutants, enhancement of replication, HIV-1, low-fitness mutants, sparsomycin

Introduction

Highly active antiretroviral therapy (HAART) has been successful in controlling the progression of AIDS caused by HIV-1. However, HAART has accelerated the emergence and spread of multidrug-resistant HIV-1. Once drug-resistant HIV-1 occurs in a HIV-1-infected patient, the success rate of HAART drops substantially. Resistance testing has been shown to be valuable to optimize HAART against HIV-1 infection (Hirsch *et al.*, 2000; Rodriguez-Rosado *et al.*, 1999). Profiling drug resistance might be necessary even before the initiation of HAART because of the spread of drug-resistant HIV-1 (Boden *et al.*, 1999; Gehringer *et al.*, 2000; Yerly *et al.*, 1999).

Genotypic and phenotypic resistance testing are the two major ways to determine the drug resistance of clinical HIV-1 isolates. For genotyping, the HIV-1 genome isolated from the infected individuals is sequenced. This HIV-1 genome is than cross-referenced with a database and we are able to predict the drug resistance profile of HIV-1. However, it is impossible to predict the phenotype when we encounter a combination of mutations that has never been documented. This may raise a concern when a new drug is released in the market. Another problem in the genotyping is the presence of genotype-phenotype discordance (Parkin *et al.*, 2003; Sarmati *et al.*, 2002).

Alternatively, for the phenotypic resistance testing, the drug resistance profiles are measured by many biological/virological assay systems (Hertogs *et al.*, 1998; Iga *et al.*, 2002; Jarmy *et al.*, 2001; Kellam & Larder, 1994; Menzo *et al.*, 2000; Walter *et al.*, 1999). Phenotypic resistance testing is powerful because the diagnosis is based on experimental observations. Among the systems, ones that depend on the multi-round HIV-1 replication seemed to provide the best drug resistance data reflecting the *in vivo* condition. However, many drug-resistant mutants have lower replication capabilities than wild-type (wt) HIV-1, which makes the phenotypic resistance testing difficult and time-consuming. In order to overcome these problems, it would be useful to develop a technique to make HIV-1

replicate faster without altering the effectiveness of antiretroviral compounds.

During our search for an inhibitor of HIV-1 replication, we found sparsomycin, a metabolite from *Streptomyces sparsogenes*, which reproducibly enhanced the replication of HIV-1. Therefore, we tested whether sparsomycin merits phenotypic drug resistance profiling studies on low-fitness HIV-1 isolates.

Materials and methods

Cells and viruses

Human embryonic kidney (HEK) 293T cells were maintained in Dulbecco's modified Eagle's medium (Sigma-Aldrich, Tokyo, Japan) supplemented with 10% fetal bovine serum (FBS; Hyclone, Logan, UT, USA), penicillin and streptomycin (Invitrogen, Carlsbad, CA, USA). H9, Jurkat, SupT1 and HPB-Ma cells were maintained in RPMI1640 (Sigma-Aldrich) supplemented with 10% FBS, penicillin and streptomycin. All the cell lines were incubated at 37°C in a humidified 5% CO_2 atmosphere. As previously described, HIV-1 (HXB2) was produced by transfecting proviral DNA into 293T cells and collecting the culture medium 3 days post-transfection (Komano *et al.*, 2004). The replication-incompetent HIV-1 (HXB2 Δ*vpr*, Δ*rev*, Δ*env*, Δ*nef*) was produced by transfecting the proviral DNA carrying renilla luciferase with the *nef* open reading frame into 293T cells, along with the expression plasmid for *env*, *tat*, *rev* and *nef* (pIIIex) as described previously in Komano *et al.* (2004). As previously described, the D30N, L90M, and D25N protease mutants of HIV-1 were generated by the site-directed mutagenesis (Sugiura *et al.*, 2002). The multidrug-resistant HIV-1 DR3577 was a clinical isolate from a patient on HAART in which reverse transciptase carried the following mutations M41L, D67N, K70R, V75M, K101Q, T215F and K219Q, and protease carried the following mutations L10I, K20R, M36I, M46I, L63P, A71V, V82T, N88S and L90M. For the generation of replication-incompetent murine leukaemia virus (MLV) vector expressing firefly luciferase, pCMMP luciferase was transfecting into 293T cells along with *gag/pol* and VSV-G expressing plasmids as described previously (Komano *et al.*, 2004).

Chemical compound

Sparsomycin was either purchased from Sigma-Aldrich (cat. S1667) or obtained from Dr Nakajima (Toyama Prefectural University, Toyama, Japan). Sparsomycin was dissolved in 2mM dimethyl sulphoxide and stored at –20°C until use.

Monitoring HIV-1 replication

For HIV-1 infection, 1×10^6 cells were incubated with the culture supernatant containing approximately 10 ng of p24. Alternatively, wt HIV-1, or D30N and L90M mutants were introduced into cells either by electroporation or DEAE-dextran-mediated protocol as previously described (Matsuda *et al.*, 1993; Miyauchi *et al.*, 2005). The culture supernatants were collected everytime the infected cells were split until they ceased to proliferate. The amount of p24 antigen of HIV-1 in the culture supernatants was quantified by using Retro TEK p24 antigen ELISA kit according to the manufacturer's protocol (Zepto Metrix, Buffalo, NY, USA). The signal was detected by Vmax ELISA reader (Molecular Devices, Palo Alto, CA, USA).

Determining 50% inhibitory concentrations (IC_{50})

IC_{50} was calculated by using a reporter cell line, MARBLE, developed by Sugiura *et al.* (personal communication). In brief, a clone of HPB-Ma carrying the long terminal repeat (LTR)-driven firefly luciferase cassette integrated in its genome was infected with HIV-1 and incubated in the presence of varying concentrations of antiretroviral compounds for a week. The cells were then lysed to measure the firefly luciferase activity, which represented the propagation of HIV-1 in culture. The firefly luciferase activity was normalized by constitutively-expressed renilla luciferase activity. The dual luciferase assay was performed according to the manufacturer's protocol (Promega, Madison, WI, USA). Chemiluminescence was detected by Lmax (Molecular Devices).

Reporter assay

The –1 frameshift reporters, pLuc (–1) and pLuc (0), were kindly provided by Dr Brakier-Gingras (Dulude *et al.*, 2002). The renilla luciferase expression vector phRL/CMV was purchased from Promega. pLTR Luc encoded GFP-luciferase under the regulation of HIV-1's LTR promoter (Komano *et al.*, 2004). pLTRΔnefLuc encoded renilla luciferase by substituting *nef* in the proviral context of HXB2 (Komano *et al.*, 2004). Plasmids were transfected into 293T cells by Lipofectamine 2000 plus reagent in accordance with the manufacturers' protocol (Invitrogen). For the detection of luciferase activities, the dual glo luciferase assay was performed at 2–3 days post-transfection or post-infection according to the manufacturers' protocol (Promega). The signal was detected by Vmax ELISA reader (Molecular Devices).

Western blot analysis

COS-7 cells were transfected with Lipofectamine 2000 (Invitrogen) or Fugen6 (Roche, Basel, Switzerland) according to the manufacturer's protocol with proviral DNA encoding the D25N protease mutant. At 48 h post-transfection, cells were washed with PBS and lysed in a buffer containing 4% SDS, 100 mM Tris-HCl (pH 6.8), 12% 2-ME, 20% glycerol and bromophenol blue.

Samples were boiled for 10 min. Protein lysates approximately equivalent to 5×10^4 cells were separated in 5–20% SDS-PAGE (Perfect NT Gel, DRC, Tokyo, Japan), transferred to a polyvinylidene fluoride (PVDF) membrane (Immobilon-P^{SQ}; Millipore, Billerica, MA, USA), and blocked with 5% dried non-fat milk (Yuki-Jirushi, Tokyo, Japan) in PBS. For the primary antibody, we used rabbit anti-*Gag* polyclonal antibody or mouse anti-*Gag* monoclonal antibody. For the secondary antibody, either a biotinylated anti-rabbit antibody or a biotinylated anti-mouse goat antibody (GE Healthcare Bio-Science, Piscataway, NJ, USA) was used. For the tertiary probe, a horseradish peroxidase-conjugated streptoavidin (GE Healthcare Bio-Science) was used. Signals were developed by incubating blots with a chemilumenescent horseradish peroxidase substrate (GE Healthcare Bio-Science) and detected by using Lumi-Imager F1 (Roche).

Results

The structure of sparsomycin, a metabolite from *Streptomyces sparsogenes,* is unique in that it comprises two unusual entities, a monooxodithioacetal moiety and a uracil acrylic acid moiety (Figure 1A). H9 cells were infected with HIV-1 and then maintained in the presence of varying concentrations of sparsomycin. Dimethyl sulphoxide was added in the absence of sparsomycin throughout this study. At 7 days post-infection, a massive syncytial formation was found in the presence of sparsomycin (Figure 1B). The higher the concentration of sparsomycin, the faster p24 accumulated in the culture supernatants (Figure 1C). Similar observations were made in Jurkat, SupT1 (Figures 1D and E), and HPB-Ma cells although the speed of p24 accumulation appeared different among the cell lines. On the other hand, sparsomycin did not show any detectable effect on the cell growth under concentrations of 500 nM.

These results could be due to sparsomycin's ability to either boost HIV-1 replication or select a mutant that replicated substantially faster than the wt HIV-1. To differentiate these possibilities, we recovered the virus-containing culture supernatants from the H9 cell culture at the peak of HIV-1 replication in the presence of 400 nM sparsomycin (asterisk in Figure 1F). Then fresh H9 cells were infected with the recovered virus, the cells were split into two samples and 400 nM of sparsomycin was added to each sample. If sparsomycin selected fast-growing mutants, the replication profiles of HIV-1 should resemble the original sample with sparsomycin (solid circle, Figure 1F) regardless of sparsomycin's presence. However, the replication profile in the presence of sparsomycin shifted leftward (Figure 1G), suggesting that it was unlikely that sparsomycin selected the fast-replicating viral mutants. Therefore, it is likely that sparsomycin boosted HIV-1 replication. Replication-enhancing effects were also seen by using the chemically-synthesized derivatives of sparsomycin (unpublished data; Nakajima *et al.*, 2003). The replication-boosting effect levelled-out at 500 nM, an approximately 20-fold lower concentration than the 50% toxic dose (TD_{50}) of sparsomycin (Ash *et al.*, 1984).

To demonstrate the usefulness of sparsomycin in HIV-1 research, we have examined whether sparsomycin can also boost the replication of drug-resistant low-fitness isolates. The D30N and L90M are common drug-resistant mutations found within HIV-1 protease in HIV-1-infected patients on HAART (Devereux *et al.*, 2001; Kantor *et al.*, 2002; Pellegrin *et al.*, 2002; Sugiura *et al.*, 2002). We introduced proviral DNA carrying the D30N or L90M mutation into H9, Jurkat, and SupT1 cells. HIV-1 replication was than monitored in the presence of 400 nM of sparsomycin. The replication of both viral mutants was substantially enhanced in the presence of sparsomycin in H9 cells (Figures 2A and B). The replication of the L90M-carrying mutant was also enhanced in Jurkat and SupT1 cells (Figures 2C and D). Of note, the replication enhancement appeared profound when HIV-1 displayed relatively slower replication kinetics (for example, the replication of D30N-carrying mutant versus the wt HIV-1 in H9 cells or the replication of HIV-1 in SupT1 versus H9 cells).

Considering the use of sparsomycin in the phenotypic resistance testing, it is critical to know whether sparsomycin affects HIV-1's sensitivity to the antiretroviral drugs. The respective IC_{50} of representative antiretroviral drugs in the absence and the presence of 400 nM sparsomycin were as follows: reverse transcriptase inhibitors; lamivudine, 13.7 and 10.4 nM, and stavudine, 6.3 and 17.0 nM; an non-nucleoside reverse transcriptase inhibitor, nevirapine, 78.2 and 146.4 nM; and protease inhibitors, nelfinavir, 2.8 and 1.0 nM, indinavir, 4.2 and 3.0 nM, and amprenavir, 3.4 and 3.3 nM. Then, we examined whether the presence of sparsomycin affected the IC_{50} of both zidovudine (AZT) and lopinavir (LPV) against a multidrug-resistant HIV-1 isolate, DR3577. The magnitude of both AZT and LPV-resistance of DR3577 was in the order of 2 log (data not shown). The IC_{50}s of AZT in the presence and absence of 400 nM sparsomycin were 14.0 and 36.7 nM, respectively, and for LPV they were 103.1 and 78.9 nM, respectively. These data suggested that the presence of sparsomycin did not significantly influence the IC_{50} of antiretroviral drugs on the replication of both wt and drug-resistant HIV-1.

Finally, we investigated the possible mechanisms that sparsomycin enhanced the replication of HIV-1 and its mutants although the estimated magnitude of enhancement per single replication cycle was small. To do this, we used non-T cells to increase the sensitivity of assays. First, we examined if the early phase of HIV-1's life cycle was

Figure 1. The enhancement of HIV-1 replication by sparsomycin

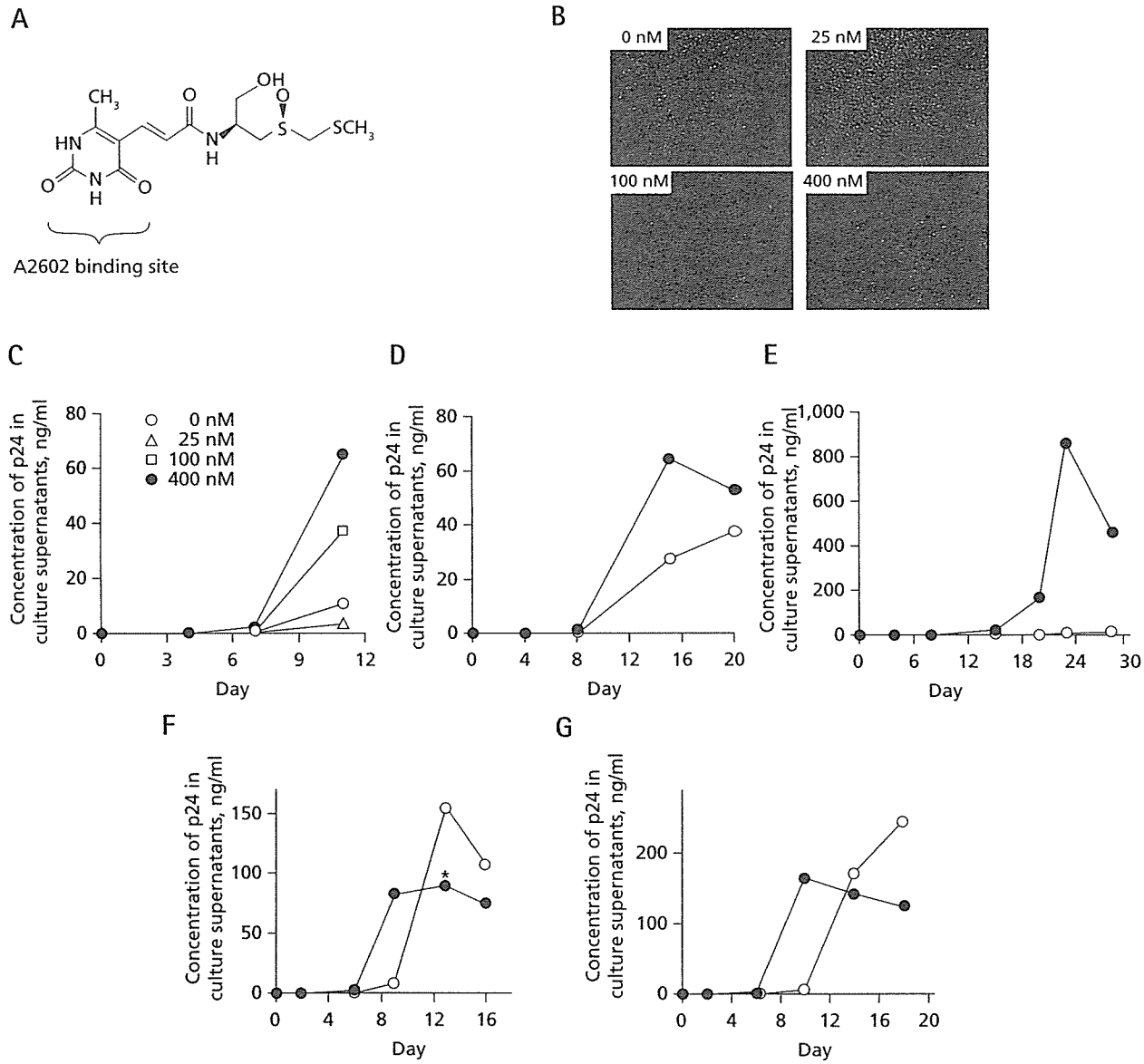

(A) Structure of sparsomycin. The uracil acrylic acid moiety confers the binding capacity to the conserved nucleobase A2602 of the large ribosomal subunit. **(B)** H9 cells infected with HIV-1 were photographed at a week after infection (magnification, ×200). **(C)** The replication profiles of HIV-1 in H9 cells in the presence of varying concentrations of sparsomycin. **(D-G)**. The replication profiles of HIV-1 in Jurkat **(D)**, SupT1 **(E)**, and H9 cells **(F and G)** in the presence of sparsomycin (400 nM, solid circle) or in the absence (open circle; **F and G**). Virus-containing culture supernatant was collected at 13 days post-infection (asterisk, **F**) to infect fresh H9 cells and the replication profiles of HIV-1 were analysed in the presence of sparsomycin (400 nM, solid circle) or in the absence (open circle, **G**).

positively affected by sparsomycin. In the presence of increasing concentrations of sparsomycin, 293 $CD4^+$ T-cells and NP2 CD4 CXCR4 cells were infected with either a replication-deficient HIV-1 vector enveloped with its own *Env* or a VSV-G-psueodotyped MLV vector. Two days post-infection, cells were lysed to measure the luciferase activities representing the efficiency of viral infection. Our results indicate that luciferase activities were not significantly increased at the replication-enhancing dose for both HIV-1 and MLV vectors (Figure 3A). Thus suggesting that the early phase of the retroviral life cycle was not detectably affected by sparsomycin.

Figure 2. Sparsomycin's ability to enhance replication of low-fitness drug resistant HIV-1 mutants

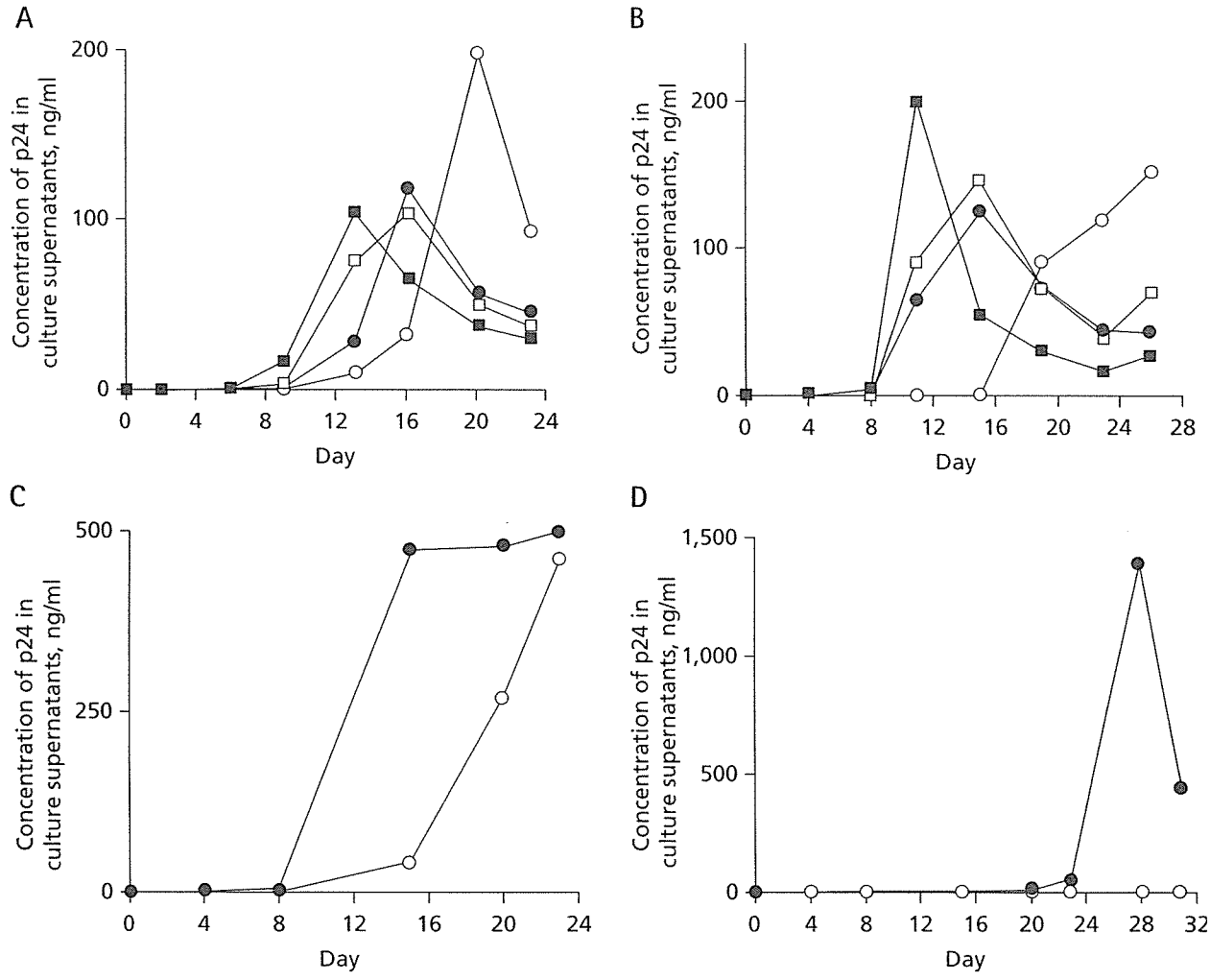

(A and B) The replication kinetics of the D30N-carrying (circle) and L90M-carrying (square) mutants in the presence of sparsomycin (400 nM, solid) or in the absence (open) were investigated twice independently in H9 cells. **(C and D)** The replication kinetics of the L90M-carrying mutant were examined in Jurkat cells **(C)** and SupT1 cells **(D)** in the presence of sparsomycin (400 nM, solid circle) or in the absence (open circle).

Next, we examined the possible active role of sparsomycin in the late phase of HIV-1's life cycle. Sparsomycin has been reported to be a potential enhancer of the −1 frameshift (Dinman *et al.*, 1997). Therefore, we tested whether sparsomycin could positively affect the efficiency of the translational −1 slip at HIV-1's frameshift signal using the reporter assay system established by Dulude *et al.* (2002). The −1 frameshift reporter was created by placing the firefly luciferase in the *pol* frame, pLuc(−1), whereas the control plasmid pLuc(0) has the luciferase in the *gag* frame after the frameshift signal (Figure 3B). In addition, HIV-1's LTR-driven luciferase reporter constructs were tested (pLTR Luc and pLTRΔnefLuc; Figure 3B). We transfected these reporter plasmids into 293T cells along with the renilla luciferase-expressing plasmid phRL/CMV (Promega) to measure the non-specific or toxic effects, if any, of sparsomycin. Cells were incubated in the presence of varying concentrations of sparsomycin for 3 days. Then the dual luciferase assay was performed. The pLuc(−1) behaved differently from the other groups in that the luciferase activities from the pLuc(−1) increased in a dose-dependent fashion. The magnitude of increasement was 2.3-fold at the replication-enhancing dose (Figure 3C). The positive correlation between the relative luciferase activity and the concentration of sparsomycin was statistically significant (r=0.926, P<0.001, n=8, Student's t-test). In contrast, the luciferase activities from the other reporters, even the renilla luciferase plasmid

co-transfected with the pLuc(-1) vector, remained unchanged (Figure 3C). These data suggested that sparsomycin positively affected the efficiency of HIV-1's –1 frameshift. It also suggested that sparsomycin did not enhance transcription from the viral promoter or the translation of proteins driven by the LTR promoter to enhance HIV-1 replication.

If the efficiency of –1 frameshift was increased, we would expect that the *Gag–Pol* to *Gag* ratio to increase. To test this, we transfected COS-7 cells with the HIV-1's proviral DNA carrying the D25N mutation in protease that produced catalytically inactive protease to increase the sensitivity of detecting *Gag–Pol* (Xie *et al.*, 1999). When sparsomycin was added, the intensities of *Gag–Pol* gradually increased in relation to the reporter assay. The *Gag–Pol* to *Gag* ratio reached 1.3-fold at 400 nM sparsomycin when normalized with results produced in the absence of sparsomycin (Figure 3D). The average and standard deviation of the *Gag–Pol* to *Gag* ratio from four independent experiments were 1.29 ± 0.14 at the replication enhancing concentration of sparsomycin (1.29-, 1.48-, 1.16-, and 1.24-fold increase). Similar results were obtained by using

Figure 3. The possible mechanism of HIV-1 replication enhancement by sparsomycin

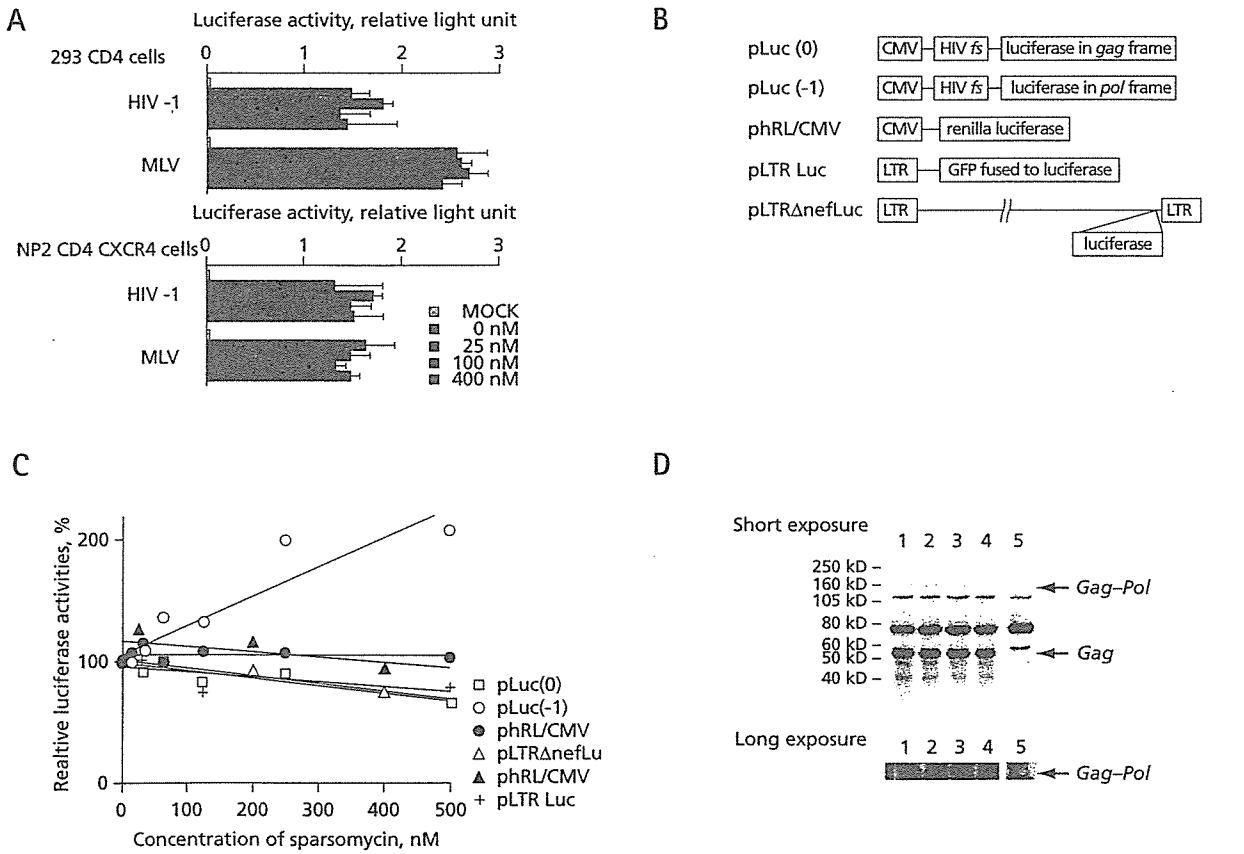

(A) The single round infection efficiencies of HIV-1 and murine lukaemia virus (MLV) vectors measured by the virally-encoded luciferase activities in 293 CD4$^+$ T-cells and NP2 CD4 CXCR4 cells in the presence of varying concentrations of sparsomycin. **(B)** The schematic drawing of constructs used in the reporter assay. The HIV-1's frameshift signal (*fs*) was placed between the CMV promoter and the luciferase. The luciferase was placed in either the *gag* frame (pLuc(0)) or the *pol* frame (pLuc(-1)). The renilla luciferase expression vector phRL/CMV was used in parallel. The pLTR Luc encodes the GFP-luciferase driven by HIV-1's LTR promoter. The pLTRΔnefLuc has the renilla luciferase substituting *nef* in the proviral context of HXB2. **(C)** The luciferase activities from the above reporter constructs without sparsomycin were set as 100% and the relative luciferase activities in the presence of sparsomycin were shown. The renilla luciferase activities from phRL/CMV were shown for the pLuc(-1) (solid circle) and pLTRΔnefLuc (solid triangle) transfections in particular. The pLuc(-1) behaved differently from the other groups and the positive correlation between the relative luciferase activity and the concentration of sparsomycin was statistically significant (r=0.926, P<0.001, n=8, Student's t-test). The SD was within 10% from the avgerage. Shown are the representative data from two independent experiments. **(D)** Western blot analysis to measure the *Gag–Pol* and *Gag* ratio. Cell extracts were separated in the SDS-polyacrylamide gel and immunoblotted by using the rabbit polyclonal antibodies raised against p24. (lane 1, 0 nM; lane 2, 20 nM; lane 3, 200 nM; lane 4, 400 nM; lane 5, MOCK). The lower panel shows the *Gag–Pol* signal obtained from the long exposure of the same blot.

two different antibodies recognizing *Gag*. We were unable to detect a significant increase in the *Env*:*Gag* ratio (unpublished data), suggesting that the sparsomycin's effect on *Gag–Pol*:*Gag* ratio was specific. These data suggested that the translational efficiencies of viral proteins were not equally enhanced by sparsomycin. Altogether, it was strongly suggested that the sparsomycin's replication-boosting effect on HIV-1 was partly due to the enhancement of the –1 frameshift efficiency.

Discussion

In the present study, we have demonstrated that sparsomycin is an enhancer of HIV-1 replication in many human T cell lines at concentrations between 400–500nM. Our preliminary observation suggested that HIV-1 replication was also enhanced in primary peripheral blood monocyte culture (data not shown). Sparsomycin should be able to accelerate the study on the low-fitness HIV-1 such as drug-resistant mutants. As sparsomycin did not alter the IC_{50} of multiple antiretroviral drugs on both wt and drug-resistant HIV-1, its usage should be able to facilitate the phenotypic resistance testing of clinical isolates and as a result, benefit HIV-1-infected patients. Our observation raised an immediate concern as to whether sparsomycin-producing Streptomyces species caused an opportunistic infection in humans, which influenced AIDS progression. However, we did not find any reports suggesting so.

Sparsomycin and puromycin are the only antibiotics that can inhibit protein synthesis in bacterial, archaeal and eukaryotic cells (Ottenheijm *et al.*, 1986; Porse *et al.*, 1999). Sparsomycin has the ability to enhance the –1 frameshift in mammalian cells as well as *S. cervisiae* (Dinman *et al.*, 1997). The proposed molecular mechanism behind this ability was either through a higher affinity of the donor stem for the ribosome and slowing down the rate of the peptidyl transfer reaction, or a change in the steric alignment between donor and acceptor tRNA stems resulting in decreased peptidyl-transfer rates. Conversely, puromycin is not known to enhance the –1 frameshift in mammalian cells. At sub-toxic concentrations, puromycin was unable to enhance the HIV-1 replication (unpublished data). These data, along with the data provided in this paper, implied that the sparsomycin's unique ability to enhance the –1 frameshift might play a role in boosting the HIV-1 replication.

The maintenance of the –1 frameshift efficiency at the optimal range is critical for HIV-1 to replicate (Jacks *et al.*, 1988). Therefore, limiting *Gag–Pol* production should lead to an inhibition of viral replication because *pol* encodes enzymes essential for viral replication (Levin *et al.*, 1993). In contrast, it was also reported that increasing the *Gag–Pol* to *Gag* ratio by twofold resulted in a reduction of viral replication (Hung *et al.*, 1998; Shehu-Xhilaga *et al.*, 2001). Thus, a modest alteration of the –1 frameshift efficiency should markedly affect the replication capacity of HIV-1. Our data indicated that sparsomycin increased the efficiency of –1 frameshift by 1.3-fold, which produces a better replication capacity for HIV-1. As a result, we hypothesize that HIV-1 has a 'suboptimal' –1 frameshift efficiency. In theory, the 1.3-fold difference per one replication cycle becomes approximately 10-fold after 10 rounds of viral replication cycle because the effect accumulates exponentially. The difference should become larger when HIV-1 replicates with the slower kinetics and the replication profile is monitored over a longer time course. In fact, our experimental data were in good agreement with the above estimation. In nature, HIV-1 does not accumulate mutations within the frameshift signal to achieve the higher frameshift efficiencies. This implies that there are multiple and complex regulatory mechanisms that keep the efficiency of the –1 frameshift at suboptimum. Under these conditions, the best efficiency of HIV-1 survival in the host might be achieved. Altogether, one of the possible mechanisms that sparsomycin boosted the HIV-1 replication could be the enhancement of the –1 frameshift efficiency.

Acknowledgements

We thank Drs Hironori Sato and Tsutomu Murakami for critical reading of the manuscript. This work was partly supported by both the Japan Health Science Foundation and the grant from Japanese Ministry of Health, Labor, and Welfare.

References

Ash RJ, Fite LD, Beight DW & Flynn GA (1984) Importance of the hydrophobic sulfoxide substituent on nontoxic analogs of sparsomycin. *Antimicrobial Agents and Chemotherapy* **25**:443–445.

Boden D, Hurley A, Zhang L, Cao Y, Guo Y, Jones E, Tsay J, Ip J, Farthing C, Limoli K, Parkin N & Markowitz M (1999) HIV-1 drug resistance in newly infected individuals. *Journal of the American Medical Association* **282**:1135–1141.

Devereux HL, Emery VC, Johnson MA & Loveday C (2001) Replicative fitness *in vivo* of HIV-1 variants with multiple drug resistance-associated mutations. *Journal of Medical Virology* **65**:218–224.

Dinman JD, Ruiz-Echevarria MJ, Czaplinski K & Peltz SW (1997) Peptidyl-transferase inhibitors have antiviral properties by altering programmed -1 ribosomal frameshifting efficiencies: development of model systems. *Proceedings of the National Academy of Sciences of the United States of America* **94**:6606–6611.

Dulude D, Baril M & Brakier-Gingras L (2002) Characterization of the frameshift stimulatory signal controlling a programmed -1 ribosomal frameshift in the human immunodeficiency virus type 1. *Nucleic Acids Research* **30**:5094–5102.

Gehringer H, Bogner JR, Goebel FD, Nitschko H & von der Helm K (2000) Sequence analysis of the HIV-1 protease coding region of 18 HIV-1-infected patients prior to HAART and possible implications on HAART. *Journal of Clinical Virology* **17**:137–141.

Hertogs K, de Bethune MP, Miller V, Ivens T, Schel P, Van Cauwenberge A, Van Den Eynde C, Van Gerwen V, Azijn H, Van Houtte M, Peeters F, Staszewski S, Conant M, Bloor S, Kemp S, Larder B & Pauwels R (1998) A rapid method for simultaneous detection of phenotypic resistance to inhibitors of protease and reverse transcriptase in recombinant human immunodeficiency virus type 1 isolates from patients treated with antiretroviral drugs. *Antimicrobial Agents and Chemotherapy* **42**:269–276.

Hirsch, MS, Brun-Vezinet F, D'Aquila RT, Hammer SM, Johnson, VA, Kuritzkes DR, Loveday C, Mellors JW, Clotet B, Conway B, Demeter LM, Vella S, Jacobsen DM & Richman DD (2000) Antiretroviral drug resistance testing in adult HIV-1 infection: recommendations of an International AIDS Society-USA Panel. *Journal of the American Medical Association* **283**:2417–2426.

Hung M, Patel P, Davis S & Green SR (1998) Importance of ribosomal frameshifting for human immunodeficiency virus type 1 particle assembly and replication. *Journal of Virology* **72**:4819-4824.

Iga M, Matsuda Z, Okayama A, Sugiura W, Hashida S, Morishita K, Nagai Y & Tsubouchi H (2002) Rapid phenotypic assay for human immunodeficiency virus type 1 protease using *in vitro* translation. *Journal of Virological Methods* **106**:25–37.

Jacks T, Power MD, Masiarz FR, Luciw PA, Barr PJ & Varmus HE. (1988) Characterization of ribosomal frameshifting in HIV-1 gag-pol expression. *Nature* **331**:280–283.

Jarmy G, Heinkelein M, Weissbrich B, Jassoy C & Rethwilm A (2001) Phenotypic analysis of the sensitivity of HIV-1 to inhibitors of the reverse transcriptase, protease, and integrase using a self-inactivating virus vector system. *Journal of Medical Virology* **64**:223–231.

Kantor R, Fessel WJ, Zolopa AR, Israelski D, Shulman N, Montoya JG, Harbour M, Schapiro JM & Shafer RW (2002) Evolution of primary protease inhibitor resistance mutations during protease inhibitor salvage therapy. *Antimicrobial Agents and Chemotherapy* **46**:1086–1092.

Kellam P & Larder BA (1994) Recombinant virus assay: a rapid, phenotypic assay for assessment of drug susceptibility of human immunodeficiency virus type 1 isolates. *Antimicrobial Agents and Chemotherapy* **38**:23–30.

Komano J, Miyauchi K, Matsuda Z & Yamamoto N (2004). Inhibiting the Arp2/3 Complex limits infection of both intracellular mature vaccinia virus and primate lentiviruses. *Mol Biol Cell* **15**:5197–5207.

Levin JG, Hatfield DL, Oroszlan S & Rein A (1993) Mechanisms of translational suppression used in the biosynthesis of reverse transcriptase. In *Reverse transcriptase*, pp. 5–31. Edited by AM Skalka & SP Goff. New York: Cold Spring Harbor Laboratory Press.

Matsuda Z, Yu X, Yu QC, Lee TH & Essex M (1993) A virion-specific inhibitory molecule with therapeutic potential for human immunodeficiency virus type 1. *Proceedings of the National Academy of Sciences of the United States of America* **90**:3544–3548.

Menzo S, Rusconi S, Monachetti A, Colombo MC, Violin M, Bagnarelli P, Varaldo PE, Moroni M, Galli M, Balotta C & Clementi M (2000) Quantitative evaluation of the recombinant HIV-1 phenotype to protease inhibitors by a single-step strategy. *AIDS* **14**:1101–1110.

Miyauchi K, Komano J, Yokomaku Y, Sugiura W, Yamamoto N & Matsuda, Z (2005) Role of the specific amino acid sequence of the membrane-spanning domain of human immunodeficiency virus type 1 in membrane fusion. *Journal of Virology* **79**:4720–4729.

Nakajima N, Enomoto T, Watanabe T, Matsuura N & Ubukata M. (2003) Synthesis and activity of pyrimidinylpropenamide antibiotics: the alkyl analogues of sparsomycin. *Bioscience, Biotechnology, and Biochemistry* **67**:2556–2566.

Ottenheijm HC, van den Broek LA, Ballesta JP & Zylicz Z (1986) Chemical and biological aspects of sparsomycin, an antibiotic from Streptomyces. *Progress in Medicinal Chemistry* **23**:219–268.

Parkin NT, Chappey C & Petropoulos CJ (2003) Improving lopinavir genotype algorithm through phenotype correlations: novel mutation patterns and amprenavir cross-resistance. *AIDS* **17**:955–961.

Pellegrin I, Breilh D, Montestruc F, Caumont A, Garrigue I, Morlat P, Le Camus C, Saux MC, Fleury HJ & Pellegrin JL (2002) Virologic response to nelfinavir-based regimens: pharmacokinetics and drug resistance mutations (VIRAPHAR study). *AIDS* **16**:1331–1340.

Porse BT, Kirillov SV, Awayez MJ, Ottenheijm HC & Garrett RA (1999) Direct crosslinking of the antitumor antibiotic sparsomycin, and its derivatives, to A2602 in the peptidyl transferase center of 23S-like rRNA within ribosome-tRNA complexes. *Proceedings of the National Academy of Sciences of the United States of America* **96**:9003–9008.

Rodriguez-Rosado R, Briones C & Soriano V (1999) Introduction of HIV drug-resistance testing in clinical practice. *AIDS* **13**:1007–1014.

Sarmati L, Nicastri E, Parisi SG, d'Ettorre G, Mancino G, Narciso P, Vullo V & Andreoni M (2002) Discordance between genotypic and phenotypic drug resistance profiles in human immunodeficiency virus type 1 strains isolated from peripheral blood mononuclear cells. *Journal of Clinical Microbiology* **40**:335–340.

Shehu-Xhilaga M, Crowe SM & Mak J (2001) Maintenance of the Gag/Gag-Pol ratio is important for human immunodeficiency virus type 1 RNA dimerization and viral infectivity. *Journal of Virology* **75**:1834–1841.

Sugiura W, Matsuda Z, Yokomaku Y, Hertogs K, Larder B, Oishi T, Okano A, Shiino T, Tatsumi M, Matsuda M, Abumi H, Takata N, Shirahata S, Yamada K, Yoshikura H & Nagai Y (2002) Interference between D30N and L90M in selection and development of protease inhibitor-resistant human immunodeficiency virus type 1. *Antimicrobial Agents and Chemotherapy* **46**:708–715.

Walter H, Schmidt B, Korn K, Vandamme AM, Harrer T & Uberla K. (1999). Rapid, phenotypic HIV-1 drug sensitivity assay for protease and reverse transcriptase inhibitors. *Journal of Clinical Virology* **13**:71–80.

Xie D, Gulnik S, Gustchina E, Yu B, Shao W, Qoronfleh W, Nathan A & Erickson JW (1999) Drug resistance mutations can effect dimer stability of HIV-1 protease at neutral pH. *Protein Science* **8**:1702–1707.

Yerly S, Kaiser L, Race E, Bru JP, Clavel F & Perrin L (1999) Transmission of antiretroviral-drug-resistant HIV-1 variants. *Lancet* **354**:729–733.

Received 5 December 2005, accepted 23 March 2006

J|A|C|S
ARTICLES
Published on Web 05/24/2006

Computational Simulations of HIV-1 Proteases—Multi-drug Resistance Due to Nonactive Site Mutation L90M

Hirotaka Ode,* Saburo Neya, Masayuki Hata, Wataru Sugiura,† and Tyuji Hoshino‡

Contribution from the Graduate School of Pharmaceutical Sciences, Chiba University, Chiba 263-8522, Japan

Received January 29, 2006; E-mail: odehir@graduate.chiba-u.jp

Abstract: Human immunodeficiency virus type 1 protease (HIV-1 PR) is one of the proteins that currently available anti-HIV-1 drugs target. Inhibitors of HIV-1 PR have become available, and they have lowered the rate of mortality from acquired immune deficiency syndrome (AIDS) in advanced countries. However, the rate of emergence of drug-resistant HIV-1 variants is quite high because of their short retroviral life cycle and their high mutation rate. Serious drug-resistant mutations against HIV-1 PR inhibitors (PIs) frequently appear at the active site of PR. Exceptionally, some other mutations such as L90M cause drug resistance, although these appear at nonactive sites. The mechanism of resistance due to nonactive site mutations is difficult to explain. In this study, we carried out computational simulations of L90M PR in complex with each of three kinds of inhibitors and one typical substrate, and we clarified the mechanism of resistance. The L90M mutation causes changes in interaction between the side chain atoms of the 90th residue and the main chain atoms of the 25th residue, and a slight dislocation of the 25th residue causes rotation of the side chain at the 84th residue. The rotation of the 84th residue leads to displacement of the inhibitor from the appropriate binding location, resulting in a collision with the flap or loop region. The difference in levels of resistance to the three inhibitors has been explained from energetic and structural viewpoints, which provides the suggestion for promising drugs keeping its efficacy even for the L90M mutant.

Introduction

Human immunodeficiency virus type 1 (HIV-1) proliferates under the assistance of its own aspartic protease, so-called HIV-1 protease (PR), in its life cycle.[1] HIV-1 PR is an enzyme composed of two identical polypeptides, each of which consists of 99 amino acid residues (Figure 1A), and has a function to process the viral Gag and Gag-Pol polyprotein precursors. Because this processing is essential for the viral maturation, the inhibition of PR function leads to an incomplete viral replication and prevents the infection of other cells.[2] Therefore, HIV-1 PR is an attractive target for anti-HIV-1 drugs. Seven PR inhibitors (PIs) have been approved by the FDA[3-9] and have successfully lowered the death rate due to acquired immune deficiency syndrome (AIDS) in advanced countries during the past decade. However, the emergence of PI-resistant mutants has become a serious problem in AIDS therapies.[10-13] The accumulation of multidrug-resistant mutations within HIV-1 PR makes it difficult to control viral replication in patients. Hence, PIs that maintain drug efficacy even for drug-resistant mutants are needed.

Most mutations causing a high level of drug resistance occur at the active site of HIV-1 PR. For example, D30N and G48V lead to specific resistance against nelfinavir (NFV) and saquinavir (SQV), respectively, and I84V shows multidrug resistance against several approved PIs.[7,10-18] Recent structural analyses by not only X-ray crystallography[19-28] but also computational

[1] AIDS Research Center, National Institute of Infectious Diseases, Musashimurayama, Tokyo 208-1011, Japan.
[‡] Also PRESTO, JST, 4-1-8 Honcho Kawaguchi, Saitama, Japan.

(1) Kräusslich, H. G.; Wimmer, E. *Ann. Rev. Biochem.* **1988**, *57*, 701.
(2) Kohl, N. E.; Emini, E. A.; Schleif, W. A.; Davis, L. J.; Heimbach, J. C.; Dixon, R. A.; Scolnick, E. M.; Sigal, I. S. *Proc. Natl. Acad. Sci. U.S.A.* **1988**, *85*, 4686.
(3) Craig, J. C.; Duncan, I. B.; Hockley, D.; Grief, C.; Roberts, N. A.; Mills, J. S. *Antiviral Res.* **1991**, *16*, 295.
(4) Vacca, J. P.; et al. *Proc. Natl. Acad. Sci. U.S.A.* **1994**, *91*, 4096.
(5) Kempf, D. J.; et al. *Proc. Natl. Acad. Sci. U.S.A.* **1995**, *92*, 2484.
(6) Livington, D. J.; Pazhanisamy, S.; Porter, D. J.; Partaledis, J. A.; Tung, R. D.; Painter, G. R. *J. Infect. Dis.* **1995**, *172*, 1238.
(7) Patick, A. K.; et al. *Antimicrob. Agents Chemother.* **1996**, *40*, 292 (Erratum, *40*, 1575).
(8) Carrillo, A.; Stewart, K. D.; Sham, H. L.; Norbeck, D. W.; Kohlbrenner, W. E.; Leonard, J. M.; Kempf, D. J.; Molla, A. *J. Virol.* **1998**, *72*, 7532.
(9) Robinson, B. S.; et al. *Antimicrob. Agents Chemother.* **2000**, *44*, 2093.
(10) Condra, J. H.; et al. *Nature (London)* **1995**, *374*, 579.
(11) Kantor, R.; Fessel, W. J.; Zolopa, A. R.; Israelski, D.; Shulman, N.; Montoya, J. G.; Harbour, M.; Schapiro, J. M.; Shafer, R. W. *Antimicrob. Agents Chemother.* **2002**, *46*, 1086.
(12) Wu, T. D.; Schiffer, C. A.; Gonzales, M. J.; Taylor, J.; Kantor, R.; Chou, S.; Israelski, D.; Zolopa, A. R.; Fessel, W. J.; Shafer, R. W. *J. Virol.* **2003**, *77*, 4836.
(13) Johnson, V. A.; Brun-Vézinet, F.; Clotet, B.; Conway, B.; Kuritzkes, D. R.; Pillay, D.; Schapiro, J.; Telenti, A.; Richman, D. *Top. HIV Med.* **2005**, *13*, 125.
(14) Patick, A. K.; Duran, M.; Cao, Y.; Shugarts, D.; Keller, M. R.; Mazabel, E.; Knowles, M.; Chapman, S.; Kuritzkes, D. R.; Markowitz, M. *Antimicrob. Agents Chemother.* **1998**, *42*, 2637.
(15) Jacobsen, H.; Yasargil, K.; Winslow, D. L.; Craig, J. C.; Krohn, A.; Duncan, I. B.; Mous, J. *Virology* **1995**, *206*, 527.
(16) Jacobsen, H.; Hänggi, M.; Ott, M.; Duncan, I. B.; Andreoni, M.; Vella, S.; Mous, J. *Antiviral Res.* **1996**, *29*, 95.
(17) Jaconsen, H.; Hänggi, M.; Ott, M.; Duncan, I. B.; Owen, S.; Andreoni, M.; Vella, S.; Mous, J. *J. Infect. Dis.* **1996**, *173*, 1379.
(18) Ermolieff, J.; Lin, X.; Tang, J. *Biochemistry* **1997**, *36*, 12364.
(19) Mahalingam, B.; Louis, J. M.; Reed, C. C.; Adomat, J. M.; Krouse, J.; Wang, Y.-F.; Harrison, R. W.; Weber, I. T. *Eur. J. Biochem.* **1999**, *263*, 238.
(20) Hong, L.; Zhang, X. C.; Hartsuck, J. A.; Tang, J. *Protein Sci.* **2000**, *9*, 1898.

10.1021/ja060682b CCC: $33.50

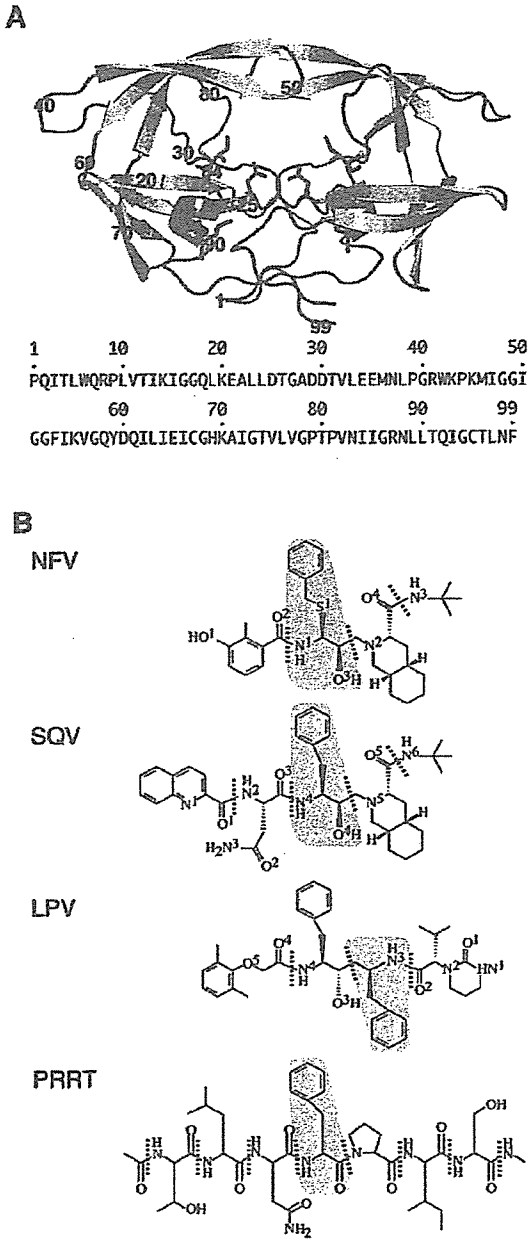

Figure 1. A: Structure of HIV-1 PR. Locations of the two catalytic aspartates, the 84th and the 90th residues, are shown in stick representation. The WT sequence of HIV-1 PR is shown below. B: Chemical structures of NFV, SQV, LPV, and PRRT. Each red dotted line shows a junction between subsites. The P1 subsite is highlighted with an orange background, and the P1′ subsite is highlighted with a yellow background.

studies[29−34] have revealed that these active site mutations changed direct interactions between PR and PI and caused unfavorable contact between them. Nonactive site mutations such as L10F and L90M have also been reported to cause a high level of resistance, although these residues cannot directly interact with PIs.[7,10−18] It is difficult to understand how nonactive site mutations lead to resistance against PIs. L90M is a primary mutation responsible for resistance against NFV and SQV.[7,14−17] L90M also appears to be associated with resistance to other PIs.[11−13] The structures of L90M PR mutants in complex with PIs have been determined through X-ray crystallographic approaches by some groups[20,26] and through our previous computational simulations.[33] These structures showed that the side chains of the mutated M90/M90′ altered their interactions with the catalytic aspartates D25/D25′. Additionally, L90M mutation affected local conformations at the 80's loop of PR, which is quite far from the location of the 90th residues. The mechanism of resistance due to L90M, however, is still not clear, and a strategy for the design of potent drugs against L90M-acquired virus has not yet been established.

In this study, we carried out computational simulations of L90M PR in complex with several kinds of ligands to clarify the mechanism of resistance due to L90M. NFV, SQV, and lopinavir (LPV) were selected as representative PI inhibitors currently used in the clinical field (Figure 1B). NFV and SQV lose their ability to inhibit PRs that have acquired L90M mutation. In contrast, single mutations have little effect on the inhibition ability of LPV.[35] In addition, the oligopeptide at the PR/RT cleavage site (PRRT) was selected as a typical substrate for the enzyme to investigate the effect of L90M on substrate binding (Figure 1B). The PR/RT cleavage site contains Phe-Pro at the P1−P1′ residues (notation by Schecter and Berger[36]). It is unusual for mammalian endopeptidases to cleave the peptide bond located at the N-terminal side of Pro, and this cleavage site is specific to HIV-1 PR.[37,38] This cleavage mechanism is unique as reported previously.[39−41] Therefore, the structure of PRRT was used as the base of drug design for NFV, SQV, and some PIs.[3,7,42] In this study, the binding energies of NFV, SQV, LPV, and PR/RT were first calculated to compare the levels of resistance of the wild type (WT) and L90M mutant. The binding structures were then compared in two groups of inhibitors: one groups consisting of HIV inhibitors that lose drug efficacy due

(21) Mahalingam, B.; Louis, J. M.; Hung, J.; Harrison, R. W.; Weber, I. T. *Proteins* **2001**, *43*, 455.
(22) Mahalingam, B.; Boross, P.; Wang, Y.-F.; Louis, J. M.; Fischer, C. C.; Tozser, J.; Harrison, R. W.; Weber, I. T. *Proteins* **2002**, *48*, 107.
(23) Weber, J.; et al. *J. Mol. Biol.* **2002**, *324*, 739.
(24) King, N. M.; Melnick, L.; Prabu-Jeyabalan, M.; Nalivaika, E. A.; Yang, S. S.; Gao, Y.; Nie, X.; Zepp, C.; Heefner, D. L.; Schiffer, C. A. *Protein Sci.* **2002**, *11*, 418.
(25) Prabu-Jeyabalan, M.; Nalivaika, E. A.; King, N. M.; Schiffer, C. A. *J. Virol.* **2003**, *77*, 1306.
(26) Mahalingam, B.; Wang, Y.-F.; Boross, P. L.; Tozser, J.; Louis, J. M.; Harrison, R. W.; Weber, I. T. *Eur. J. Biochem.* **2004**, *271*, 1516.
(27) King, N. M.; Prabu-Jeyabalan, M.; Nalivaika, E. A.; Wigerinck, P.; Béthune, M. P.; Schiffer, C. A. *J. Virol.* **2004**, *78*, 12012.
(28) Prabu-Jeyabalan, M.; Nalivaika, E. A.; King, N. M.; Schiffer, C. A. *J. Virol.* **2004**, *78*, 12446.
(29) Rick, S. W.; Topol, I. A.; Erickson, J. W.; Burt. S. K. *Protein Sci.* **1998**, *8*, 1750.
(30) Piana, S.; Carloni, P.; Rothlisberger, U. *Protein Sci.* **2002**, *11*, 2393.
(31) Clemente, J. C.; Hemrajani, R.; Blum, L. E.; Goodenow, M. M.; Dunn, B. M. *Biochemistry* **2003**, *42*, 15029.
(32) Perryman, A. L.; Lin, J.-H.; McCammon, J. A. *Protein Sci.* **2003**, *13*, 1108.
(33) Ode, H.; Ota, M.; Neya, S.; Hata, M.; Sugiura, W.; Hoshino, T. *J. Phys. Chem. B* **2005**, *109*, 565.
(34) Wittayanarakul, K.; Aruksakunwong, O.; Saen-oon, S.; Chantratita, W.; Parasuk, V.; Sompornpisut, P.; Hannongbua, S. *Biophys. J.* **2005**, *88*, 867.
(35) Kempf, D. J.; Isaacson, J. D.; King, M. S.; Brun, S. C.; Xu, Y.; Real, K.; Bernstein, B. M.; Japour, A. J.; Sun, E.; Rode, R. A. *J. Virol.* **2001**, *75*, 7462.
(36) Schechter, I.; Berger, A. *Biochem. Biophys. Res. Commun.* **1967**, *27*, 157.
(37) Pearl, L. H.; Taylor, W. R. *Nature (London)* **1987**, *328*, 482.
(38) Darke, P. L.; Nutt, R. F.; Brady, S. F.; Garsky, V. M.; Ciccarone, T. M.; Leu, C.-H.; Lumma, P. K.; Freidinger, R. M.; Veber, D. F.; Sigal, I. S. *Biochem. Biophys. Res. Commun.* **1988**, *156*, 297.
(39) Okimoto, N.; Tsukui, T.; Hata, M.; Hoshino, T.; Tsuda, M. *J. Am. Chem. Soc.* **1999**, *121*, 7349.
(40) Okimoto, N.; Tsukui, T.; Kitayama, K.; Hata, M.; Hoshino, T.; Tsuda, M. *J. Am. Chem. Soc.* **2000**, *122*, 5613.
(41) Okimoto, N.; Kitayama, K.; Hata, M.; Hoshino, T.; Tsuda, M. *J. Mol. Struct. (THEOCHEM)* **2001**, *543*, 53.
(42) Roberts, N. A.; et al. *Science* **1990**. *248*, 358.

to L90M mutations, such as NFV and SQV, and the other group consisting of drugs that maintain efficacy, such as LPV. Prominent differences between the two groups were seen at the contact of M90 to D25, shifts of D25, rotation of the side chains of I84, displacement of the flap region of I50, and deformation of the loop region of P81. D25, I84, I50, and P81 are all located at the active site of the PR. Detail discussion are developed in contrast with the resistivity of PR. Our findings provide information for designing better inhibitors that maintain drug efficacy despite L90M or other nonactive site mutations.

Materials and Methods

Molecular Dynamics Simulation. Before carrying out molecular dynamics (MD) simulations, quantum chemical calculations were executed for PIs to deduce the atom charges utilized in MD simulations. Geometry optimization was performed on each PI, and the electrostatic potential was calculated at the B3LYP/6-31G(d,p) level using the Gaussian03 program.[43] The partial atom charges were determined using the RESP method[44] so that the atom charges could reproduce the values of the calculated electrostatic potential at the surrounding points of the PI. Charges were set equal between two atoms if they were the same element and had the same bond coordination. Minimizations and MD simulations were carried out using the Sander module of the AMBER7 package.[45] The AMBER ff02 force field[46] was used as the parameters for van der Waals and bonded energy terms basically, and the general AMBER force field[47] was used as the parameters for NFV, SQV, and LPV.

Each initial structure for the clade B HXB2 PRs in complex with NFV, SQV, and LPV was modeled from the atom coordinates of the X-ray crystal structure (PDB code: 1OHR,[48] 1HXB,[42,49] and 1MUI,[50] respectively) using the LEaP module (Figure 1A). The initial structure for the PR in complex with PRRT before the catalytic reaction was modeled in the same manner as that previously reported.[39] The oligopeptide of ACE-THR-LEU-ASN-PHE-PRO-ILE-SER-NME was utilized as PRRT, and one water molecule was inserted between PRRT and D25/D25′. Each model was placed in a rectangular box filled with about 8000 TIP3P water molecules,[51] with all of the crystal water molecules remaining. One water molecule was added between LPV and I50/I50′ in the LPV complex model, because no crystal water molecule was present in the crystallographic data. It is known that the hydrogen bonds between PI and I50/I50′ via the water molecule are critically important for PI binding with HIV-1 PR.[33,39–41] The cutoff distance for the long-range electrostatic and the van der Waals energy terms was set at 12.0 Å. All covalent bonds to hydrogen atoms were constrained using the SHAKE algorithm.[52] Periodic boundary conditions were applied to avoid edge effects in all calculations. Energy minimization was achieved in three steps. At first, movement was allowed only for the water molecules and ions. Next, the ligand and the mutated residues were allowed to move in addition to the water molecules and ions. Finally, all atoms were permitted to move freely. In each step, energy minimization was executed by the steepest descent method for the first 1000 steps and the conjugated gradient method for the subsequent 3000 steps. After 52.0 ps heating calculation until 300 K using the NVT ensemble, 1.5 ns equilibrating calculation was executed at 1 atm and at 300 K using the NPT ensemble, with an integration time step of 1.0 fs. In the present calculations, the MD simulations showed no large fluctuations after about 500 ps equilibrating calculation (Supporting Information Fig. S1). Hence, atom coordinates were collected at the interval of 0.5 ps for the last 500 ps to analyze the structure in detail.

Protonation States. The protonation states of catalytic aspartates D25 and D25′ vary depending on the binding inhibitors or substrates. Hence, the appropriate protonation states of catalytic aspartates should be determined for the respective ligands. For NFV, the protonated state was already determined in our previous study.[33] That is, D25 was protonated and D25′ was unprotonated in each of WT PR and L90M PR in complex with NFV. To determine the protonation states when SQV or LPV binds to the WT PR, the total energies of the two kinds of complexes were compared after energy minimization. One complex represented a combination of protonated D25/unprotonated D25′ states, and the other represented the opposite combination. This comparison clearly suggested the preference of the protonated D25 and unprotonated D25′ states (Supporting Information Table S1 A). In contrast to the case of WT PR, we used another method to determine the protonation states of L90M PR with SQV or LPV because they might have greatly different conformation from the respective crystal structures. Hence, we executed 1.5 ns MD simulations of the two protonation states in these models and compared the total energies of the two protonation states for the last 500 ps of the simulations. The energy comparison indicated that L90M PR in complex with each of SQV and LPV preferred the protonated D25 and unprotonated D25′ states (Supporting Information Table S1 B). For both WT and L90M PR with PRRT, the D25 unprotonated and D25′ protonated states were selected so that the hydrolysis reaction could proceed as described in a previous paper.[39]

Binding Energy Calculation (MM/PBSA). The binding free energy[53] was calculated by the following equation:

$$\Delta G_b = \Delta G_{MM} + \Delta G_{sol} - T\Delta S$$

where ΔG_b is the binding free energy in solution, ΔG_{MM} is the molecular mechanics (MM) interaction energy, ΔG_{sol} is the solvation energy, and $-T\Delta S$ is the contribution of conformational entropy to the binding. Since the contribution of conformational entropy to the change of ΔG_b is negligible among the mutants as pointed out by Massova,[54] the last entropy term in the energy estimation was neglected. ΔG_{MM} was calculated by the following equation:

$$\Delta G_{MM} = \Delta G_{int}^{ele} + \Delta G_{int}^{vdw}$$

where ΔG_{int}^{ele} and ΔG_{int}^{vdw} are electrostatic and van der Waals interaction energies between a ligand and a protein. These energies were computed using the same parameter set as that used in the MD simulation, and no cutoff was applied for the calculation. Solvation energy ΔG_{sol} can be divided into two parts:

$$\Delta G_{sol} = \Delta G_{sol}^{ele} + \Delta G_{sol}^{nonpol}$$

The electrostatic contribution to the solvation free energy (ΔG_{sol}^{ele}) was calculated by the Poisson–Boltzmann (PB) method using the DelPhi program.[55] The hydrophobic contribution to the solvation free energy (ΔG_{sol}^{nonpol}) was determined with a function of the solvent-accessible surface-area.[56]

Hydrogen Bond Criterion. The formation of a hydrogen bond was defined in terms of distance and orientation. The combination of donor

(43) Frisch, M. J.; et al. *Gaussian 03*; Gaussian, Inc., Wallingford CT, 2004.
(44) Cieplak, P.; Cornell, W. D.; Bayly, C.; Kollman, P. A. *J. Comput. Chem.* **1995**, *16*, 1357.
(45) Case, D. A.; et al. *AMBER 7*; University of California: San Francisco, 2002.
(46) Wang, J.; Cieplak, P.; Kollman, P. A. *J. Comput. Chem.* **2000**, *21*, 1049.
(47) Wang, J.; Wolf, R. M.; Caldwell, J. W.; Kollman, P. A.; Case, D. A. *J. Comput. Chem.* **2004**, *25*, 1157.
(48) Kaldor, S. W.; et al. *J. Med. Chem.* **1997**, *40*, 3979.
(49) Krohn, A.; Redshaw, S.; Ritchie, J. C.; Graves, B. J.; Hatada, M. H. *J. Med. Chem.* **1991**, *34*, 3340.
(50) Stoll, V.; et al. *Bioorg. Med. Chem.* **2002**, *10*, 28032.
(51) Jorgensen, W. L.; Chandrasekhar, J.; Madura, J. D.; Impey, R. W.; Klein, M. L. *J. Chem. Phys.* **1983**, *79*, 926.
(52) Ryckaert, J.-P.; Ciccotti, G.; Berendsen, H. J. C. *J. Comput. Phys.* **1977**, *23*, 327.
(53) Kollman, P. *Chem. Rev.* **1993**, *93*, 2395.
(54) Massova, I.; Kollman, P. A. *Perspect. Drug. Discovery Des.* **2000**, *18*, 113.
(55) Honig, B.; Nicholls, A. *Science* **1995**, *268*, 1144.
(56) Sitkoff, D.; Sharp, K. A.; Honig, B. *J. Phys. Chem.* **1994**, *98*, 1978.

Table 1. Binding Energies of Each Model[a]

		ΔG_{int}^{elp}	ΔG_{int}^{vdw}	ΔG_{sol}	ΔG_b[b]	ΔG_b[c]	resistant level[d]
NFV	WT	−24.4 ± 3.6	−66.6 ± 3.6	37.5 ± 3.3	−53.5 ± 4.2	+2.8	5
	L90M	−20.2 ± 3.8	−64.1 ± 3.1	33.6 ± 3.5	−50.7 ± 4.6		
SQV	WT	−29.6 ± 4.7	−71.5 ± 4.0	34.7 ± 3.6	−66.4 ± 5.2	+2.7	3.5
	L90M	−27.9 ± 4.2	−72.9 ± 3.8	37.1 ± 3.6	−63.7 ± 4.7		
LPV	WT	−31.2 ± 4.8	−71.1 ± 3.7	41.0 ± 3.4	−61.8 ± 4.5	−0.3	~1
	L90M	−29.8 ± 5.2	−74.1 ± 3.2	41.9 ± 3.4	−62.1 ± 4.9		
PRRT	WT	−74.7 ± 9.3	−84.1 ± 4.2	91.7 ± 5.3	−67.2 ± 7.5	−0.5	-
	L90M	−72.4 ± 6.3	−84.7 ± 4.7	89.4 ± 4.7	−67.7 ± 5.4		

[a] Energy is presented in units of kcal/mol. [b] $T\Delta S$ is not included. [c] $\Delta\Delta G_b = \Delta G_b$(L90M) − ΔG_b(WT) [d] Resistance level was taken from refs 7, 18, and 35. Resistance level is defined as IC90(L90M)/IC90(WT) or as IC50(L90M)/IC50(WT) in the references.

D, hydrogen H, and acceptor A atoms with a D−H···A configuration was regarded as a hydrogen bond when the distance between donor D and acceptor A was shorter than R_{max}(= 3.5 Å) and the angle H−D−A was smaller than Θ_{max}(= 60.0°).

Results

Binding Energy Calculations. The influence of L90M mutation on binding energy ΔGb was examined for each ligand. Table 1 shows the results of MM/PBSA calculations for the WT and L90M PR in complex with each ligand. L90M reduced the binding energies of NFV and SQV. Results of some experiments have suggested that L90M mutation caused resistance against these inhibitors.[7,11−18] On the other hand, L90M PR exhibits almost the same affinity as that of WT PR for LPV. It has been reported that the affinity of LPV was hardly affected by any single mutations.[35] Hence, the results of our simulations are compatible with the results of previous experimental analyses. The affinity of L90 M PR with PRRT is almost the same as that of WT PR.

Hydrogen Bonds between PR and Ligands. Hydrogen bonds play an essential role in stabilizing protein−ligand complexes. We examined 1000 snapshots during the last 500 ps and identified direct or one water molecule-mediated hydrogen bonds (Supporting Information Table S2). NFV mainly creates hydrogen bonds with D25′ and D30 in the WT model. In contrast, NFV interacts with D25 and D25′ in L90M PR. That is, NFV hardly interacts with D30 in the L90M model. It is known that D30 contributes significantly to PR−NFV binding and that the mutation D30N causes specific resistance against NFV.[7,14,57,58] Moreover, in WT and L90M PR, one water molecule is located between I50/I50′ and NFV. This water molecule creates hydrogen bonds with I50′ of WT PR (99.8% of the bonds being maintained during the last 500 ps of simulation) and with I50 of L90M PR (92.4%), while these hydrogen bonds are often broken with NFV in each model (~50%). SQV has a direct interaction with D25′ and a one water molecule-mediated interaction with I50′ in both WT and L90M models. In addition, the main chain at the P2 subsite of SQV makes a hydrogen bond with G48 in both models. In contrast, the side chain at the P2 subsite (−$CONH_2$) interacts with different residues in the two models. The side chain interacts with G48 in the WT model and with D30 in the L90M model. Interestingly, G48 is a residue whose mutation causes specific resistance against SQV.[15−18] Thus, both NFV and SQV lose significant hydrogen bonds due to L90M mutation. On the other hand, LPV has similar hydrogen bond networks in the WT and L90M models. LPV creates direct hydrogen bonds with D25, D25′, and D29. One water molecule connects LPV to the 50th residues by hydrogen bonding. PRRT has similar interactions with D29, D30, and G48 in S4−S1 pockets in the WT and L90M models. However, PRRT has different interactions in S1′-S4′ pockets. One water molecule also stays between D25/D25′ and PRRT in the PR model, while it hardly makes any stable hydrogen bond.

Comparison of the Structures of the WT and L90M Models. To clarify the effect of mutation at the 90th residue on active site conformation, the average structure of the L90M model for the last 500 ps was compared with that of the corresponding WT model. The L90M model was fitted to the WT model using the coordinates of the main chain atoms N, Cα, and C, and the root-mean-squared deviation (RMSD) value was calculated (Figure 2). When the structures of each ligand in the WT and L90M models were compared, some atoms of NFV and SQV were found to exhibit large RMSD values (>2.0 Å). Atoms at the thio-phenol group (−S−C_6H_5) in NFV are dislocated to a quite different position, and all of the atoms in SQV are shifted in the same direction. On the other hand, no atoms in LPV exhibit such large RMSD values. In the case of PRRT, the P4−P1′ subsites have almost identical conformations, but there is a prominent difference at the P2′-P4′ subsite. The tertiary structures of the WT PR and L90M PR were also compared. RMSD 3D plots clearly indicate that deviation in the NFV complex model is markedly large compared to other ligand-bound cases. In the case of NFV, main chain atoms at the flap and at P79′ and its neighboring residues show large differences in WT PR and L90M PR. We previously reported conformational changes at the same residues.[33] There are small differences between the results of the present study and those of the previous study regarding the residues at the flap region. Namely, the flap region shows larger deviation from the WT in the present calculation. This is because the residues are flexible (Supporting Information Figure S2) and we examined larger sets of coordinates in this study (1000 sets of coordinates from 1 to 1.5 ns) than the previous study (200 sets of coordinates from 0.9 to 1.0 ns). L90M PR in complex with SQV shows local conformational changes at P81 and its neighbors. In the case of LPV, the main chain atoms at the active site are hardly affected by L90M mutation, although some atoms at the nonactive site show large deviations. In the case of PRRT, the main chain atoms at I50′ and its neighbors show noticeable deviations.

Mechanism of Conformational Changes at the Active Site. Figure 2 shows that L90M mutation affects the location of the

(57) Sugiura, W.; et al. *Antimicrob. Agents Chemother.* **2002**, *46*, 708
(58) Sugiura, W.; et al. *Jpn. J. Infect. Dis.* **1999**, *52*, 175.

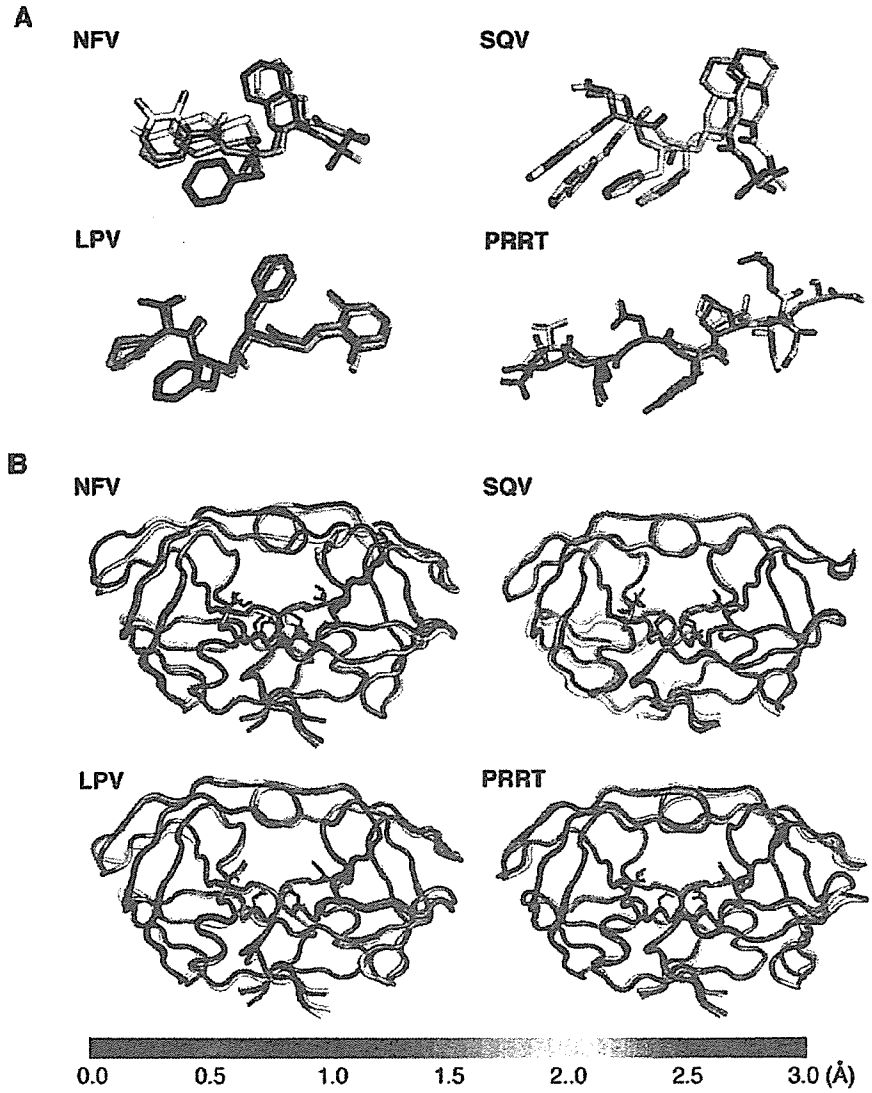

Figure 2. 3D plots of RMSD between the average structures of WT and L90M models. A: Ligands in the L90M model are shown as colored sticks. B: PRs in the L90M model are shown in colored tube representation, and D25/D25′ and I84/I84′ are shown in stick representation. The color means the magnitude of RMSD shown in the bottom bar. The L90M model was fitted on the WT model using the coordinates of main chain atoms N, Cα, and C of PR. The superimposed gray sticks and tubes represent the structure of the WT model.

ligand and the tertiary conformation of the active site of PR. To determine the reason for induction of these conformational changes at the active site by the nonactive site mutation L90M, conformations of the catalytic triad D25T26G27/D25′T26′G27′ have been examined in detail. These residues have van der Waals contacts with the side chains of the 90th residues[20,26,33] and are located at the active site. In NFV, SQV, and PRRT complex models, some residues showed about 1.0 Å deviations between WT and L90M PR (Supporting Information Table S3). On the other hand, the deviations of all of these residues in the LPV complex model are about 0.5 Å. These residues are the least fluctuating residues in PR because they create rigid hydrogen bond networks, so-called fireman grips[59] (Supporting Information Fig. S2). The root-mean-squared fluctuations (RMSF) of these residues were about 0.3 Å. Thus, these

(59) Strisovsky, K.; Tessmer, U.; Langner, J.; Konvalinka, J.; Kräusslich, H-G *Protein Sci.* **2000**, *9*, 1631

Table 2. Distances between D25 Cβ-D25′ Cβ, D25 Cβ-I84 Cβ, and 25′ Cβ-I84′ Cβ[a]

D25Cβ-D25′Cβ	NFV	SQV	LPV	PRRT
WT	6.2 ± 0.1	6.7 ± 0.2	7.1 ± 0.2	7.3 ± 0.3
L90M	6.5 ± 0.2	6.2 ± 0.1	7.0 ± 0.2	7.6 ± 0.2
Δ[b]	0.3	−0.5	0.1	0.3
D25Cβ-I84Cβ	NFV	SQV	LPV	PRRT
WT	5.6 ± 0.2	5.0 ± 0.2	4.7 ± 0.2	4.4 ± 0.3
L90M	5.0 ± 0.3	5.1 ± 0.2	4.9 ± 0.2	4.4 ± 0.3
Δ[b]	−0.6	0.1	0.2	0.0
D25′Cβ-I84′Cβ	NFV	SQV	LPV	PRRT
WT	4.4 ± 0.2	5.4 ± 0.4	5.2 ± 0.2	5.0 ± 0.2
L90M	5.8 ± 0.3	5.8 ± 0.2	5.2 ± 0.2	5.1 ± 0.2
Δ[b]	1.4	0.4	0.0	0.1

[a] Distances are presented in units of Å. [b] Difference between L90 M and WT.

conformational changes at these triads are critically important. In the case of NFV, SQV, and PRRT complex models, D25 Cβ -D25′ Cβ distances are also different between the WT and

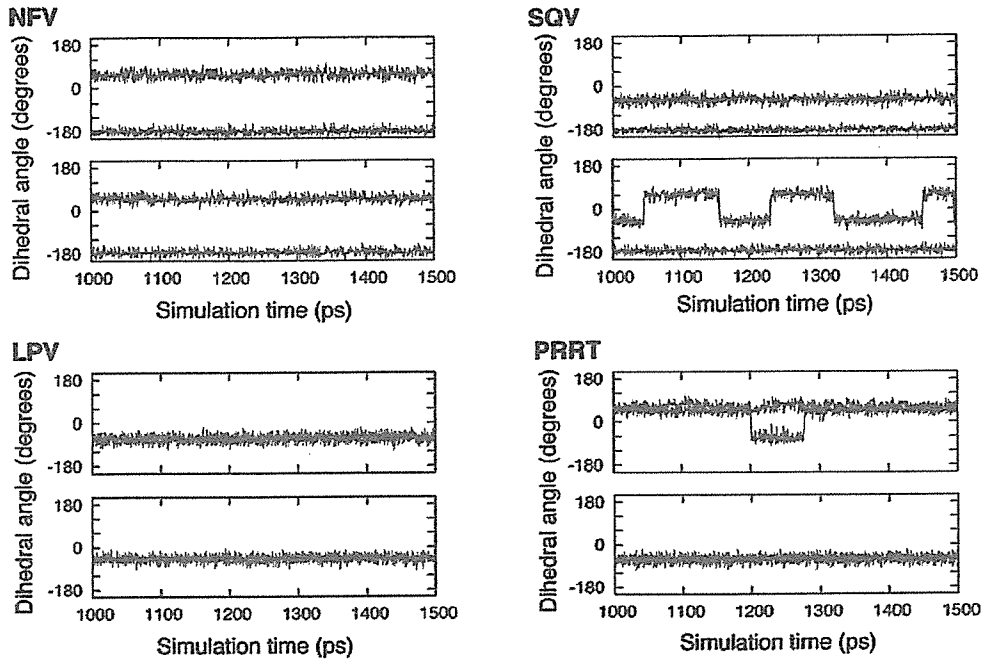

Figure 3. Dihedral angles of N−Cα−Cβ−Cγ1 of I84 (upper) and I84′ (lower) during the last 500 ps of simulations. Red lines represent the WT model, and green lines represent the L90M model.

L90M models (Table 2). There is a particularly large difference in orientations of the side chains of D25/D25′. Furthermore, in the case of NFV and SQV, rotations occur at the side chains of I84/I84′, which are active site residues and are in contact with the side chains of D25/D25′ (Figure 3). The rotations are correlated with the changes in distances between D25 Cβ and I84 Cβ and between D25′ Cβ and I84′ Cβ. That is, the rotations are induced by displacements of the catalytic aspartates D25 and D25′. The side chains of I84/I84′ have large hydrophobic contacts with the ligands, and the structure of the active site is deformed asymmetrically. Consequently, we speculate that the following mechanism causes the active site conformational changes. First, L90M mutation changes the interaction between the 90th residues and D25/D25′. Second, D25/D25′ is shifted. Third, I84/I84′ show rotations of their side chains. Finally, the interaction between ligands and I84/I84′ causes conformational changes of the active site.

Discussion

In HIV-1 PR, the 90th residue is located at the dimer interface, that is, out of the substrate-binding pocket. Hence, it has no direct contact with any ligand of PR. Despite its location, L90M mutation causes resistance against FDA-approved PIs, such as NFV and SQV.[7,11−18] It is difficult to imagine the mechanism of resistance due to L90M mutation. Several X-ray crystal structures have ever been provided for L90M PR.[20−22,26] These structures showed that the side chains of the mutated M90/M90′ altered the interactions with the catalytic aspartates D25/D25′. Hong et al. determined the crystal structure of G48V/L90M HIV-1 PR in complex with SQV. They proposed that alteration in the interactions between the 90th residues and D25/D25′ led to reduction of structural flexibility at the main chains of the catalytic triads and lowered the possibility of these main chains making structural adjustments to SQV.[20] Mahalingam et al. determined the structure of L90M HIV-1 PR in complex with IDV and with substrate analogue inhibitors. They further analyzed kinetic characteristics of L90M mutants and reported that L90M appeared to indirectly lower the dimer stability.[21,22,26] Our recent study in which computational simulations of HIV-1 PR in complex with NFV were carried out suggested that L90M mutation caused a decrease of binding energies and that conformational changes appeared at the flap and 80's loop regions, which are distant from the 90th residues.[33] Hence, for NFV, we concluded that the drug resistance due to L90M was caused by these active site conformational changes. Despite the accumulation of these experimental and theoretical findings, there has been no clear suggestion for drug designs to reduce the degree of or prevent the drug resistance due to L90M.

In this study, investigations of L90M PR were carried out for the purpose of establishing a strategy for promising drug design, and the structures of L90M PR in complexes with NFV, SQV, LPV, and a substrate at the PR/RT cleavage site (PRRT) were analyzed in detail. NFV and SQV lose their inhibitory efficacy for L90M mutation.[7,14−18] In contrast, LPV hardly changes its affinity with PR despite the L90M mutation.[35] The substrate PRRT has a unique sequence, Phe-Pro, at P1/P1′ subunits, whose structure is the basis for the drug design for NFV, SQV, and other PIs.[3,42] In all computed models, changes in interaction between catalytic aspartates D25/D25′ and the 90th residues occur due to the L90M mutation. In contrast, different responses have been observed at the active site of PR in the models. In the L90M PR/NFV complex, L90M causes large conformational changes at the active site, especially at the flap and 80's loop regions of PR. The L90M mutation also causes dislocations of side chains of D25/D25′ and rotations of side chains of I84/I84′. In the L90M PR/SQV complex, a positional shift of SQV and local conformational change at 80's loop